american physiological society
JOURNAL OF APPLIED PHYSIOLOGY

J Appl Physiol 137: 233–253, 2024.
First published June 13, 2024; doi:10.1152/japplphysiol.00243.2024

RESEARCH ARTICLE

Mitochondrial function in lungs of rats with different susceptibilities to hyperoxia-induced acute lung injury

Pardis Taheri,[1] Devanshi D. Dave,[1] Ranjan K. Dash,[1,3] Guru P. Sharma,[5] Anne V. Clough,[1,2,6] Elizabeth R. Jacobs,[2,4] and Said H. Audi[1,2,4]

[1]*Department of Biomedical Engineering, Medical College of Wisconsin, Marquette University, Milwaukee, Wisconsin, United States;* [2]*Research Service, Clement J. Zablocki V.A. Medical Center, Milwaukee, Wisconsin, United States;* [3]*Department of Physiology, Medical College of Wisconsin, Milwaukee, Wisconsin, United States;* [4]*Division of Pulmonary and Critical Care Medicine, Medical College of Wisconsin, Milwaukee, Wisconsin, United States;* [5]*Department of Radiation Oncology, Medical College of Wisconsin, Milwaukee, Wisconsin, United States; and* [6]*Department of Mathematical and Statistical Sciences, Marquette University, Milwaukee, Wisconsin, United States*

Abstract

Adult rats exposed to hyperoxia (>95% O_2) die from respiratory failure in 60–72 h. However, rats preconditioned with >95% O_2 for 48 h followed by 24 h in room air acquire tolerance of hyperoxia (H-T), whereas rats preconditioned with 60% O_2 for 7 days become more susceptible (H-S). Our objective was to evaluate lung tissue mitochondrial bioenergetics in H-T and H-S rats. Bioenergetics was assessed in mitochondria isolated from lung tissue of H-T, H-S, and control rats. Expressions of complexes involved in oxidative phosphorylation (OxPhos) were measured in lung tissue homogenate. Pulmonary endothelial filtration coefficient (K_f) and tissue mitochondrial membrane potential ($\Delta\psi_m$) were evaluated in isolated perfused lungs (IPLs). Results show that ADP-induced *state 3* OxPhos capacity (V_{max}) decreased in H-S mitochondria but increased in H-T. $\Delta\psi_m$ repolarization time following ADP-stimulated depolarization increased in H-S mitochondria. Complex I expression decreased in H-T (38%) and H-S (43%) lung homogenate, whereas complex V expression increased (70%) in H-T lung homogenate. $\Delta\psi_m$ is unchanged in H-S and H-T lungs, but complex II has a larger contribution to $\Delta\psi_m$ in H-S than H-T lungs. K_f increased in H-S, but not in H-T lungs. For H-T, increased complex V expression and V_{max} counter the effect of the decrease in complex I expression on $\Delta\psi_m$. A larger complex II contribution to $\Delta\psi_m$ along with decreased V_{max} and increased K_f could make H-S rats more hyperoxia susceptible. Results are clinically relevant since ventilation with ≥60% O_2 is often required for extended periods in patients with acute respiratory distress syndrome (ARDS).

NEW & NOTEWORTHY We assessed lung tissue mitochondrial bioenergetics in rats with tolerance (H-T) or susceptibility (H-S) to hyperoxia-induced ARDS. Results from studies in isolated mitochondria, tissue homogenate, and isolated perfused lungs show that mitochondrial bioenergetics are differentially altered in H-T and H-S lungs suggesting a potential role for mitochondrial bioenergetics in hyperoxia-induced ARDS. Results are clinically relevant since hyperoxia exposure is a primary therapy for patients with ARDS, and differential sensitivity to hyperoxia surely occurs in humans.

acute lung injury; acute respiratory distress syndrome; isolated lung mitochondria; isolated perfused lungs; lung tissue mitochondrial bioenergetics

INTRODUCTION

Acute respiratory distress syndrome (ARDS) is a life-threatening disorder characterized by refractory hypoxemia (1). This condition is one of the most frequent causes of admission to medical intensive care units, occurs in ~200,000 patients in the United States per year, and carries a mortality rate of nearly 30–40% despite the best supportive care (1–4). Lower morbidity and mortality rates should be achieved by developing clinical means for risk stratification, early detection, and novel therapies to supplement supportive care.

A primary therapy for patients with ARDS is exposure to high fractions of oxygen (O_2) (hyperoxia) to improve blood oxygenation and maintain the functions of vital organs (5). Although lifesaving, exposure to hyperoxia can cause lung injury, amplifying the damage that leads to ARDS (6–9). For most animals, prolonged exposure to >95% O_2 is lethal due to lung injury (9–12). Rat exposure to hyperoxia is a well-established model of human ARDS (9, 12). Adult rats exposed to >95% O_2 die from respiratory failure in 60–72 h (12). However, unlike other rodents, adult rats can be preconditioned to become more tolerant or more susceptible to the otherwise lethal effects of further exposure to >95% O_2 (10, 12, 13). For instance, rats preconditioned by exposure to >95% O_2 for 2 days followed by a 24-h "rest period" in room air acquire tolerance (H-T) of the otherwise lethal effects of

Correspondence: S. H. Audi (said.audi@marquette.edu).
Submitted 3 April 2024 / Revised 10 June 2024 / Accepted 11 June 2024

further exposure to >95% O_2 (13). This is evidenced by the fact that if transferred back to a >95% O_2 they survive for longer period of time (13). In contrast, adult rats exposed to 60% O_2 for 7 days become more susceptible to hyperoxia (H-S) as their survival time in subsequent exposure to a >95% O_2 decreases significantly, with the median lethal time (LT50) dropping from ~66 h for normoxia rats to ~46 h for H-S rats (14). These rat models provide a platform for assessing the underlying mechanisms of rat tolerance of, or susceptibility to, hyperoxia-induced ARDS. Differential sensitivity to hyperoxia surely occurs in humans, given the wide spectrum of responses to a similar insult (15). There is ample evidence that oxidative stress, mitochondrial dysfunction, and inflammation play key roles in hyperoxia-induced ARDS, with the pulmonary capillary endothelium a primary and early target (16–23). However, the cellular pathways that regulate these injury processes and the role of those pathways in rat tolerance or susceptibility to hyperoxia-induced ARDS are poorly understood.

Increase in the permeability of the lung air-blood barrier can lead to edema, which is a cardinal feature of ARDS (2). Previously, Bongard et al. (22) established a connection between pulmonary mitochondrial bioenergetics and lung barrier function as measured by the endothelial filtration coefficient (K_f). Specifically, they showed that inhibiting mitochondrial complex I, which decreased lung total maximum ATP content by ~80%, increased K_f by ~2.8-fold. Furthermore, the addition of coenzyme Q_1 (a homolog of endogenous ubiquinone) fully reversed the effect of rotenone (Rot) on ATP and K_f, demonstrating a key role for mitochondrial ATP in lung barrier function and a potential role for mitochondrial dysfunction in the pathogenesis of ARDS (22).

Few studies have assessed the changes in tissue mitochondrial functions in the lungs of H-T and H-S rats and the underlying mechanisms of tolerance and susceptibility (14, 24–26). Studies of mitochondrial bioenergetics in the lungs of H-S and H-T rats are needed to further our understanding of the role of mitochondrial function in the tolerance of H-T rats and the susceptibility of H-S rats to lethal hyperoxia exposure. Thus, the objective of this study was to test the hypothesis that lung mitochondrial processes are differentially altered between H-S and H-T rats compared with control (normoxia) rats. Lung tissue mitochondrial function is assessed in isolated mitochondria, tissue homogenate, and isolated perfused lungs (IPLs), i.e., a vertically integrated experimental approach to increase scientific rigor. In addition, we measure the levels of mitochondrial damage-associated molecular patterns (mt-DAMPs) in plasma and the endothelial filtration coefficient in isolated perfused lungs.

MATERIALS AND METHODS

Materials

Antibodies were purchased from Sigma-Aldrich (Cat. No. ABN-302) for mitochondrial complex I and from Thermo Fisher Scientific (Cat. No. 45-8099) for mitochondrial complexes II–V. HEK-Blue hTLR9 cells were obtained from InvivoGen (Cat. No. hkb-htlr9). Rhodamine 6G (R6G), dye tetramethylrhodamine methyl ester (TMRM), verapamil hydrochloride, carbonyl cyanide 4-(trifluoromethoxy) phenylhydrazone (FCCP), rotenone (Rot), thenoyltrifluoroacetone (TTFA), and all other reagents used in experiments were purchased from Sigma-Aldrich (St. Louis, MO).

Rat Exposure to Hyperoxia with and without Preconditioning

All treatment protocols were approved by the Institutional Animal Care and Use Committees of the Clement J. Zablocki Veterans Administration Medical Center, Medical College of Wisconsin, and Marquette University.

Adult male Sprague Dawley rats were obtained from Charles River and randomized into three groups. For normoxia (control) studies, rats [342 ± 5 (SE) g, $n = 34$] were housed in chambers with room air. Another group of rats (342 ± 5 g, $n = 26$) were housed in the exposure chambers with >95% O_2 for 48 h, followed by exposure to room air for 24 h (H-T). The third group of rats (304 ± 3 g, $n = 28$) were housed in the exposure chamber with 60% O_2 for 7 days (H-S).

Plasma mt-DAMPs Using Toll-Like Receptor 9 Assay

Exposure of cells overexpressing Toll-like receptor 9 (TLR9) receptors can be used to quantify mt-DAMPs released from damaged mitochondria in vivo (27, 28). HEK-Blue hTLR9 cells (InvivoGen, Cat. No. hkb-htlr9) were grown and used according to the manufacturer's protocol. Plasma harvested at euthanasia from individual rats was plated in 96-well dishes with the HEK-Blue cells overnight. Ligand-bound TLR9 in these cells activates an inducible secreted embryonic alkaline phosphatase reporter, turning the media blue. Color was quantified with a spectrophotometer at 620 nm.

Histology

In a randomly selected subset of rats from each group, excised lungs were fixed after inflation in 10% neutral buffered formalin (Fisher Scientific, Pittsburg, PA) and embedded in paraffin. Whole mount sections of lung were cut (4 μm thick) and stained with hematoxylin and eosin (H&E, Richard Allan, Kalamazoo, MI). Then, using high-resolution jpeg images of the slides, an investigator masked to the treatment groups obtained six representative images from preselected areas of each lung on each slide, avoiding large vessels or airways. These images were then scored independently and the six values for each rat averaged for a single "*n*." A 0–2 scoring system was used for neutrophil influx, edema, and thickness of the diffusion barrier (Table 1), as previously presented (29).

Mitochondrial Complexes I–V Expressions Using Western Blot Analysis

For complex I expression, primary antibody from Sigma-Aldrich (Cat. No. ABN-302) was used (30). This antibody recognizes NADH-ubiquinone oxidoreductase protein in complex I. The protein is a 75-kDa subunit of complex I that catalyzes electron transfer from NADH. The OxPhos Rodent WB Antibody Cocktail (Thermo Fisher Scientific, Cat. No. 45-8099) of primary antibodies was used to quantify complex II through V expression (27).

Approximately 50 mg of lung tissue was homogenized in 500 μL of Radio-Immunoprecipitation Assay (RIPA) buffer.

Table 1. *Histological scoring table on 0–2 scale*

Histology Score	Neutrophilic Influx	Edema	Alveolar Septum Thickness
0	None to very rare	None to very rare	≤1.8 × control thickness
1	Perivascular or peribronchiolar only	Proteinaceous material in >5% and <20% field	>1.8 and <2.5 × control thickness
2	Intra-alveolar and widely distributed	Proteinaceous material in >20% field	>2.5 × control thickness

After centrifugation for 10 min at 10,000 *g* to remove debris, supernatants were denatured at 80°C for 5 min. Thirty micrograms (30 μg) protein/lane were loaded for electrophoresis. The primary OxPhos and complex I antibodies were diluted 1:250 in nonfat dry milk and Tris-buffered saline -Tween 20 (TBST). After electrophoretic separation and washing, matched secondary antibodies were applied, and blots were visualized using ECL Plus detection reagent.

Complex I blots were cut at 50 kDa. The higher molecular weight bands were probed for complex I (75 kDa) and the lower molecular weight bands for β-actin (42 kDa). For the OxPhos cocktail, membranes were stripped and probed for β-actin (Sigma-Aldrich, Cat. No. A2228) after quantification of bands consistent with mitochondrial complexes II through V.

Molecular weight (MW) markers (ladder) were run with every Western blot. BioRad Precision Plus Protein Standards (Cat. No. 161-0394) or Spectra MultiColor broad range protein ladder (Cat. No. 26634, Thermo Fisher) were used for MW ladders. All comparisons of normoxia to H-T or H-S Western blot densities represent three or more separate blots. Individual data points depict biological rather than technical replicates.

For a given lane and protein, the protein density was estimated by ImageJ software and was normalized to the corresponding β-actin density. This resulting value is referred to as the "relative protein." Finally, to reduce the variability in the data from study to study, including any differences in exposure time, each immunospecific relative protein value was expressed as a fold change relative to the mean of the normoxia values from the same blot. See Supplemental Fig. S6.

Isolation of Mitochondria from Lung Tissue

For isolation of mitochondria from rat lungs, we used a modified version of a previously described approach (24, 31). In brief, rats were anesthetized, after which the chest was opened and blood was heparinized (1 mL/kg via left ventricle). The lungs were then washed free of blood with 25 mL of cold perfusion buffer (10 mM HEPES in saline with 5.5 mM glucose, pH 7.4), after which time the lungs were isolated and transferred to a petri dish on ice with 3 mL ice-cold homogenization buffer (200 mM mannitol, 10 mM HEPES, 70 mM sucrose, 1 mM EGTA, 2% fatty acid-free bovine serum albumin (BSA), and protease inhibitor at 50 μL/g lung tissue, pH 7.4) and chopped into small pieces as quickly as possible. The lung pieces along with the homogenization buffer were then transferred to a glass homogenization tube on ice for manual homogenization using pestle A (15 strokes) followed by pestle B (20 strokes). The homogenized tissue was then transferred to a chilled 50-mL cold conical tube along with additional homogenization buffer (12 mL/g lung tissue). The homogenate in the conical tube was then centrifuged at 2,000 *g* at 4°C for 15 min, and the supernatant was collected and centrifuged at 17,800 *g* at 4°C for 15 min. The resulting supernatant was removed, and the remaining pellet was resuspended in 5 mL ice-cold homogenization solution without the protease inhibitor and centrifuged at 17,800 *g* at 4°C for 15 min. The resulting supernatant was removed, and the final pellet was resuspended in 0.3–0.4 mL ice-cold isolation buffer (200 mM mannitol, 10 mM HEPES, 70 mM sucrose, and 1 mM EGTA, pH 7.4) and stored on ice to be used for the mitochondrial bioenergetic studies described in subsequent sections. Mitochondrial protein concentration was determined using BSA as the standard with Bio-Rad Quick Start Bradford Assay Kit in a Thermo Scientific NanoDrop One^C spectrophotometer (32).

To explore mitochondrial metabolic pathways potentially contributing to hyperoxic lung injury, we measured mitochondrial bioenergetics, including mitochondrial O_2 consumption rates and membrane potential ($\Delta\psi_m$) as described in the following sections.

Mitochondrial O_2 Consumption Rate

Mitochondrial respiration was measured using an Oxygraph-2k (O2K) system (Oroboros Instruments, Innsbruck, Austria) with two different experimental protocols. For the first protocol (Fig. 1*A*), a fixed ADP concentration (100 mM) was used to assess *states 2*, *3*, and *4* oxygen consumption rates (OCRs) and respiratory control ratio (RCR, *state 3* OCR/*state 2* OCR). For the second protocol (Fig. 1*B*), the dependency of *state 3* OCR on ADP concentration was assessed via the addition of sequentially increasing ADP concentrations ranging from 12.5 μM to 100 μM (33). For both protocols, the respiratory buffer (RB) contained (in mM) 130 KCl, 5 K_2HPO_4, 20 MOPS, 1 EGTA, and 0.1% bovine serum albumin at pH 7.2 adjusted with KOH, and the measurements were carried out at 37°C. Before each experiment, RB was first added to the O2K chambers (2 mL), and O_2 concentration in the RB was equilibrated for up to 15 min with air at 37°C until a stable signal was obtained at an O_2 concentration of ∼205 μM, after which the chambers' lids were closed. The experiment was initiated at $t = 0$ min with the addition of different substrate combinations at saturating concentrations, including pyruvate + malate (P + M; 10 + 5 mM), glutamate + malate (G + M; 10 + 5 mM), or succinate ± rotenone (Suc ± Rot; 7 mM ± 0.5 μM). *State 2* respiration was initiated with the addition of mitochondria (0.125 mg/mL) at time = 2 min. For the first protocol (Fig. 1*A*), *state 3* respiration was initiated at time = 5 min with the addition of ADP (100 μM). *State 4* respiration data were collected for several minutes following the phosphorylation of added ADP to ATP, after which the experiment was ended. For the second protocol (Fig. 1*B*), *state 3* respiration was initiated with the sequential addition of incremental concentrations of ADP ranging from 12.5 μM at time = 5 min to 100 μM at time = 14 min. *State 4* respiration data were collected for several minutes following the phosphorylation of the last dose of ADP (100 μM) added, after which the experiment was ended.

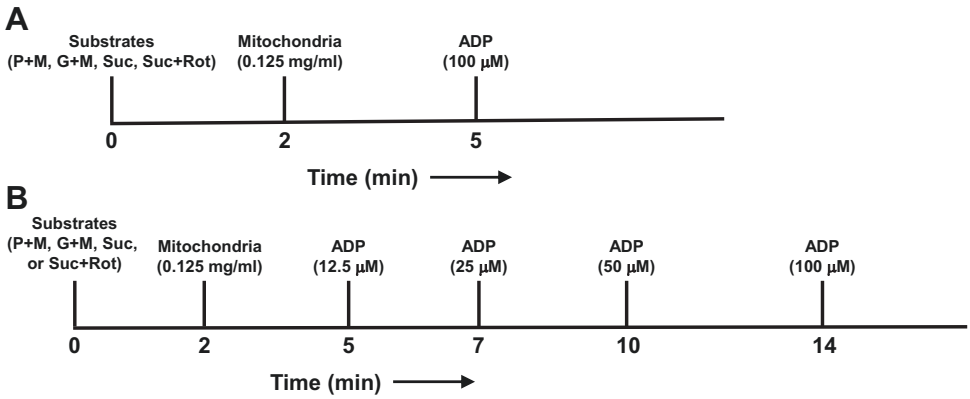

Figure 1. Addition of a single ADP concentration (*A*) and sequentially increasing ADP concentrations (*B*) protocols and timelines for the isolated mitochondria studies. P + M, pyruvate + malate; G + M, glutamate + malate; Suc, succinate; Suc + Rot, succinate + rotenone.

Oxygen consumption rate (OCR) during each of the states of respiration was calculated as the negative of the time derivative of O_2 concentration measured in the closed O2k chambers and expressed as nmol of O_2/min/mg protein (33). Data were acquired every 1 s, and 5 data points averaging was used to calculate the slope of the O_2 concentration data using the DatLab 7 software. For a given substrate combination, the respiratory control ratio (RCR) was calculated as *state 3* OCR/*state 2* OCR, measured from the collected OCR data using the first protocol (Fig. 1*A*). The calculated RCR with P + M as substrates was used to assess the functional integrity of isolated mitochondria.

Mitochondrial Membrane Potential

The Oroboros O2K system allows for the measurement of mitochondrial OCR and/or mitochondrial membrane potential ($\Delta\psi_m$) using the cationic dye TMRM (1 μM, excitation/emission wavelength 530 ± 21 nm/592 ± 22 nm), which is sequestered in the mitochondrial matrix driven by $\Delta\psi_m$ (34). Thus, $\Delta\psi_m$ was measured using the protocol in Fig. 1*B* as described in the previous section for OCR measurements with sequentially increasing ADP concentrations in the presence of different substrate combinations at 37°C. The measured TMRM emission signal at a given time was normalized by the initial TMRM signal obtained prior to the addition of mitochondria to the O2K chambers. This protocol was carried out in the lungs from normoxia ($n = 11$), H-T ($n = 6$), and H-S ($n = 5$) rats.

Isolated Perfused Rat Lung Preparation

Each rat was anesthetized with ketamine/xylazine (80–100 mg/kg:5–10 mg/kg ip). The trachea was surgically isolated and cannulated, the chest opened and heparin (0.7 IU/g body wt) injected into the right ventricle as previously described (35). The pulmonary artery and the pulmonary venous outflow were accessed via cannulas, then the heart/lungs were removed en bloc and connected to a ventilation-perfusion system. The Krebs-Ringer bicarbonate perfusate contained (in mM) 4.7 KCl, 2.51 $CaCl_2$, 1.19 $MgSO_4$, 2.5 KH_2PO_4, 118 NaCl, 25 $NaHCO_3$, and 5.5 glucose. To maintain consistent oncotic pressure, the perfusate also contained either 5% bovine serum albumin (BSA) for the K_f studies or 0.5% BSA plus 2.5% Ficoll for the $\Delta\psi_m$ studies (35, 36). The perfusion system was primed with the perfusate maintained at 37°C and equilibrated with 15% O_2, 6% CO_2, balance N_2 gas mixture resulting in perfusate P_{O_2}, P_{CO_2} and pH of ~105 Torr, 40 Torr, and 7.4, respectively. The lung was ventilated at 40 breaths/min with the aforementioned gas mixture with end-inspiratory and end-expiratory pressures of ~6 and 3 mmHg, respectively. The pulmonary artery and airway pressures were referenced to atmospheric pressure at the level of the left atrium and monitored continuously during the course of the experiment. The K_f and tissue $\Delta\psi_m$ of the isolated perfused lungs were then assessed as described in the following sections.

Pulmonary Vascular Endothelial Filtration Coefficient

Randomly selected rats from the normoxia and H-S groups were anesthetized with pentobarbital sodium (50–100 mg/kg ip). The lungs were then cannulated and removed from the thorax as aforementioned, then suspended from a calibrated force displacement transducer (F30 Type 372; Hugo Sachs Elektronik-Harvard Apparatus), which is part of a rat lung ventilation-perfusion system; lung weight was monitored continuously. The value of K_f, a measure of vascular permeability, was then determined using the approach previously described (22, 24). K_f was previously measured in the lungs from H-T rats (24). Rat lungs used for K_f studies were not used for other studies.

Mitochondrial Membrane Potential in IPL Using the Fluorescent Rhodamine 6G Dye

The single-pass perfusion system was primed with the perfusate, and ~30 mL of the perfusate was passed through the system until the lungs were clear of blood with the pump flow rate set at 10 mL/min.

The experimental protocol to probe $\Delta\psi_m$ in intact lungs was developed by Audi et al. (23, 35). It consists of three single-pass phases: a loading phase during which the lung perfusate contained R6G (0.25 μM) and the multi-drug efflux pump P-glycoprotein (Pgp) inhibitor verapamil (100 μM), a washing phase in which the R6G-free perfusate contained just verapamil, and an uncoupling phase in which the R6G-free perfusate contained the uncoupler FCCP (67 μM) with verapamil. Before each phase, the pump flow was stopped, and the reservoir was emptied and then refilled with the appropriate perfusate. For each phase, a reservoir sample was collected before restarting the flow. For the loading phase, the lung was perfused for 10 min at 10 mL/min during which venous effluent perfusate samples were

collected as previously described (23). For the washing phase, the lungs were perfused for 5 min during which venous effluent samples were collected as previously described (23). For the uncoupling phase, the lungs were perfused for 7 min during which venous effluent samples were collected as previously described (23). All collected samples were centrifuged to remove cellular components and debris (23, 35). The sample supernatant was then transferred to plastic cuvettes to measure R6G emission fluorescence (525 nm excitation/565 nm emission) using a RatioMaster fluorescence system (Photon Technology International, HORIBA Scientific, New Jersey) (23). The R6G emission signal was then converted to R6G venous effluent concentration using a standard curve (23). At the end of each experiment, the lungs were weighed, dried, and reweighed to obtain their dry weight. The aforementioned protocol was carried out in the lungs from normoxia ($n = 5$), H-T ($n = 5$), and H-S ($n = 4$) rats.

The aforementioned protocol was then repeated in the lungs from separate groups of rats with either rotenone (complex I inhibitor, 40 μM) or TTFA (complex II inhibitor, 20 μM) added to the perfusate for all three phases and to perfusate that was recirculated through the lungs prior to the start of the aforementioned three-phase protocol. For both inhibitors, the protocol was carried out in the lungs from normoxia ($n = 8$), H-T ($n = 8$), and H-S ($n = 10$) rats.

For each experimental day, a standard curve was obtained and used to convert R6G emission signal in collected samples to R6G concentrations as previously described (23). The standard curve was repeated in the presence of either rotenone or TTFA.

Statistical Analysis

Statistical evaluation of data was carried out using SigmaPlot v. 12.0 (Systat Software Inc., San Jose, CA). The level of statistical significance was set at 0.05 for all tests. For normally distributed data, group results are expressed as means ± SE. To evaluate the differences among the three groups of rats, one-way ANOVA with Tukey's post hoc analysis, or nonparametric equivalent (one-way ANOVA on ranks with Dunn's post hoc analysis) when data were not normally distributed, was used. A paired or unpaired two-tailed *t* test was used when appropriate.

DATA ANALYSIS

OCR Data from Isolated Mitochondria Studies

For the first mitochondrial O_2 consumption protocol (fixed ADP concentration, Fig. 1*A*), *state 2* OCR was estimated as the average over a 30-s period just before the addition of ADP, whereas *state 4* OCR was the average over the last 30 s of measurement (after steady state is reached). *State 3* OCR was estimated as the average OCR of a 30-s period around the maximal OCR.

For the second mitochondrial O_2 consumption protocol with sequentially increasing ADP concentrations (Fig. 1*B*), maximum *state 3* OCR for a given ADP concentration was determined. For a given group of rats, to assess the capacity and affinity of *state 3* OCR for ADP, we fit the following modified Michaelis–Menton equation to maximal *state 3* OCR as a function of added ADP concentration for the different combinations of substrates studied (33).

$$\mathrm{OCR} = V_0 + \frac{V_{\max}[\mathrm{ADP}]}{K_m + [\mathrm{ADP}]} \quad (1)$$

where V_0 = *state 2* OCR, V_{max} is a measure of the capacity of *state 3* respiration for ADP, and K_m is a measure of the affinity of *state 3* respiration for ADP.

The model fitting was carried out in MATLAB (MathWorks Inc.) using the "lsqcurvefit" function to implement the trust-region-reflective algorithm, an iterative optimization algorithm that readily incorporates bounds on the values of the parameters.

Previous studies have defined the respiratory control ratio (RCR) as either the ratio of *state 3* oxygen consumption rate (OCR) to *state 2* OCR or the ratio of *state 3* OCR to *state 4* OCR in the presence of the complex V inhibitor oligomycin (referred to as *state 4o* OCR) (33, 37–41). *State 2*, which is OCR in the presence of exogenously added substrates and no added ADP, is a measure of proton leak; *state 3*, which is OCR in the presence of exogenously added substrates and excess ADP, is a measure of mitochondrial oxidative phosphorylation (OxPhos) capacity (ATP generation capacity); *state 4*, which is OCR in the presence of exogenously added substrates following the full conversion of added ADP to ATP, is a measure of proton leak plus ATP hydrolysis activity due to recycling of some ATP back to ADP due to high ATP/ADP ratio. As such, *state 4* OCR is normally higher than *state 2* OCR. Oligomycin inhibits complex V and ATP synthesis/hydrolysis. As such, *state 4o* OCR approaches *state 2* OCR (38). Thus, *state 2* OCR is a good approximation of *state 4o* OCR (38) and does not require the addition of oligomycin. This is critically important since the use of oligomycin can cause contamination that would limit experimental protocols with the Oroboros system without extensive cleaning. For these reasons and to be consistent with our previous publications (33, 40, 41), we defined RCR as *state 3* OCR/*state 2* OCR.

Computational Model for Quantitative Interpretation of R6G Data from Isolated Perfused Lungs

For mechanistic and quantitative interpretation of the R6G dynamic data from isolated perfused lungs, we used a previously developed physiologically based pharmacokinetic (PBPK) model (23, 35). The PBPK model (see APPENDIX and Fig. 2) includes four regions, namely the tubing connecting the reservoir to the pulmonary artery, lung vasculature, extravascular (intracellular, nonmitochondrial) region, and mitochondria. The model accounts for the dominant vascular and tissue processes that determine the lung uptake and retention of R6G on passage through the pulmonary circulation, including electrochemical gradients that drive R6G from the vascular region to the extravascular region and from the extravascular to the mitochondrial region (23, 35).

The volumes of the four regions, the dissociation constant for R6G binding to protein (bovine serum albumin, BSA) in the vascular region, the mitochondrial permeability-surface area product for R6G, and the plasma membrane potential were fixed to previously estimated values (23). In addition, the rate of efflux of R6G via Pgp pump from cytoplasm to the

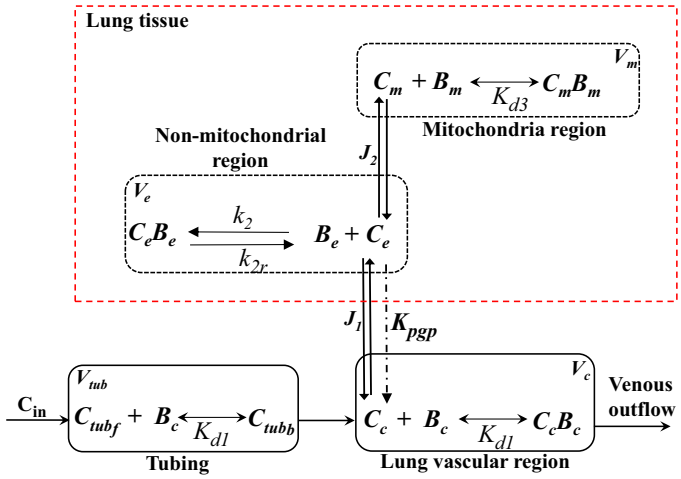

Figure 2. Physiologically based pharmacokinetic (PBPK) model of rhodamine 6G (R6G) lung uptake and retention on passage through the rat pulmonary circulation. The model consists of four regions: tubing, vascular, extravascular (nonmitochondrial), and mitochondrial with volumes V_{tub}, V_c, V_e, and V_m, respectively. [C_{in}] and [C_{tub}] are total [free (f) + bound (b)] concentration of R6G in reservoir and tubing regions, respectively; K_{d1} is the R6G to bovine serum albumin (BSA, B_c) binding dissociation constant; and [C_c] and [C_cB_c] are the respective concentrations of free and BSA-bound R6G within the vascular region; $J_1 = \frac{\alpha P_1 \Delta\psi_p}{(1-e^{-\alpha\Delta\psi_p})}\left(e^{-\alpha\Delta\psi_p}[C_c] - [C_e]\right)$, where $\alpha = ZF/RT$ is a constant dependent on the universal gas constant (R), Faraday's constant (F), R6G valence ($Z = 1$), and absolute temperature (T); [C_e] is the free R6G concentrations in the nonmitochondrial region; [B_e] and [C_eB_e] are concentrations of protein and protein-bound R6G within the nonmitochondrial region; P_1S_1 is R6G permeability-surface area product across the plasma membrane, where S_1 is the vascular surface area; $\Delta\psi_p$ is plasma membrane potential; K_{pgp} is the rate of efflux of R6G via P-glycoprotein (Pgp) pump from cytoplasm to the vascular region; k_2 is the rate constant for R6G-B_e binding within the nonmitochondrial region, and k_{2r} is the dissociation rate constant of R6G-B_e binding within the nonmitochondrial region; $J_2 = \frac{\alpha P_2 \Delta\psi_m}{(1-e^{-\alpha\Delta\psi_m})}\left(e^{-\alpha\Delta\psi_m}[C_e] - [C_m]\right)$, where $\Delta\psi_m$ is the mitochondrial membrane potential, P_2S_2 is the mitochondrial permeability-surface area product for R6G, and [C_m] is the free R6G concentrations in the mitochondrial region; K_{d3} is R6G and B_m is binding dissociation constant, where [B_m] is the protein concentration within the mitochondrial region.

vascular region was set to zero since the Pgp inhibitor verapamil was added to the perfusate for all three phases of the protocol in all experiments (23). Thus, the unknown model parameters $\Delta\psi_m$, K_{d3}, $\hat{k}_2$, k_{2r}, and P_1S_1 (see Table 2 for definition of each parameter) for the different rat groups and experimental conditions were estimated as follows. For each treatment group (normoxia, H-T, and H-S), the model solution was simultaneously fit to the mean R6G concentration data in the absence and presence of the complex II inhibitor TTFA with the values of the unknown parameters K_{d3}, $\hat{k}_2$, k_{2r}, and P_1S_1 assumed to be the same for both experimental conditions, but with different $\Delta\psi_m$ values in the absence and presence of TTFA. Thus, a total of six parameters were estimated using a Monte Carlo approach in which the model solution was fit simultaneously to the mean R6G data measured without and with the complex II inhibitor. The fitting was repeated 100 times with random initial parameter values sampled from a uniform distribution with mean within ±30% of the mean of the optimal values previously estimated from normoxia lungs (23). The model fitting was done in MATLAB (MathWorks Inc.) using "lsqcurvefit" and "ode45" to solve the differential equations numerically at each iteration. For a given group, the model solution was then fit separately to the mean R6G data measured in the presence of the complex I inhibitor rotenone since in addition to inhibiting complex I, rotenone affects the binding of R6G within the cytoplasm and mitochondria regions (23). Thus, a total of five parameters (K_{d3}, $\hat{k}_2$, k_{2r}, P_1S_1, and $\Delta\psi_m$) were estimated using the Monte Carlo approach described earlier in this paragraph. The estimated values of the model parameters are shown in Table 2. The Monte Carlo approach was also used to estimate 95% confidence intervals (Table 2) for the estimated values of the various parameters (23). For n independently estimated values of a given parameter (μ), sort the estimates from smallest to largest, then an estimate of the 95% confidence interval ($\alpha = 0.025$) for μ is provided by the estimated values that correspond to the rounded jth and kth sorted values where $j = (n + 1)\alpha$ and $k = (n + 1)(1 - \alpha)$.

RESULTS

Body Weights and Lung Wet/Dry Weight Ratios

H-S rats gained body weight over the 7-day exposure period (from 306 ± 3 to 366 ± 5 g) at a rate (8.6 g/day) similar to that of normoxia rats (25, 26). The body weights of H-T rats decreased by 3% (from 342 ± 5 to 331 ± 5 g) during the 48-h exposure period to >95% O_2, then increased by 1.6% (from 331 ± 5 to 336 ± 4 g) after the 24-h rest period in room air.

Table 3 shows no significant difference in the lung wet weight among the three groups of rats. Table 3 also shows that the lung wet/dry weight ratios for H-T and H-S rats were not significantly different from those for normoxia rats.

Histology

Figure 3 shows images of representative lung sections stained with H&E. Figure 3*A* shows the lacy architecture, single-cell alveolar septum thickness, and no evidence of neutrophil infiltration or edema, typical of normoxia lungs. Figure 3*B* shows a scant to modest collection of proteinaceous material in perivascular and intra-alveolar space in the lungs of an H-S rat, along with greater septum thickness and neutrophil infiltration. Figure 3*C* shows no evidence of neutrophil infiltration or edema and only a moderate increase in the thickness of the alveolar septum in the lungs of an H-T rat. As such, injury scores (Table 3) from the images are higher for the H-S lungs than for the normoxia lungs, with more neutrophils, edema, and alveolar thickness.

Lung Vascular Endothelial Filtration Coefficient

Table 3 shows that K_f increased by 177% in the lungs from H-S rats compared with normoxia rats. Previously, we reported that K_f for H-T lungs was not different than normoxia lungs (24).

Plasma mt-DAMPs

Table 3 shows that plasma mt-DAMPS concentrations were ~40% lower in plasma from H-T rats than normoxia rats. There were no significant differences in mt-DAMPs plasma concentrations between normoxia and H-S rats.

Table 2. *Estimated values of model parameters for each of the different experimental conditions*

Experimental Condition	$\hat{k}_2$, min^{-1}	k_{2r}, min^{-1}	K_{d3}	$\Delta\psi_m$, mV	P_1S_1, mL/min
Normoxia	9.63 ± 0.93 (8.06, 11.54)	0.109 ± 0.016 (0.083, 0.141)	0.0138 ± 0.0008 (0.0125, 0.0153)	−147.3 ± 10.7 (−132.0, −165.4)	52.1 ± 10.1 (38.1, 68.9)
Normoxia + TTFA	9.63 ± 0.93 (8.06, 11.54)	0.109 ± 0.016 (0.083, 0.141)	0.0138 ± 0.0008 (0.0125, 0.0153)	−141.6 ± 10.6 (−125.8, −156.7)	52.1 ± 10.1 (38.1, 68.9)
Normoxia + Rot	**4.70 ± 0.71** **(4.05, 6.35)**$^{\&}$	**0.064 ± 0.009** **(0.053, 0.083)**$^{\&}$	**0.0055 ± 0.0009** **(0.005, 0.008)**$^{\&}$	**−56.9 ± 2.8** **(−51.0, −63.4)**$^{\&}$	54.5 ± 8.9 (38.1, 69.0)
H-S	8.79 ± 0.80 (7.49, 10.39)	0.101 ± 0.014 (0.08, 0.131)	0.0139 ± 0.0009 (0.0125, 0.0159)	**−149.6 ± 9.0** **(−135.7, −168.9)**	55.5 ± 8.6 (39.0, 69.6)
H-S + TTFA	8.79 ± 0.80 (7.49, 10.39)	0.101 ± 0.014 (0.08, 0.131)	0.0139 ± 0.0009 (0.0125, 0.0159)	**−124.6 ± 6.5** **(−116.1, −137.8)**	55.5 ± 8.6 (39.0, 69.6)
H-S + Rot	**7.70 ± 1.05** **(6.35, 9.72)***	0.095 ± 0.015 (0.076, 0.124)	**0.0069 ± 0.0005** **(0.0062, 0.008)**$^{\&}$	**−72.0 ± 4.0** **(−66.6, −80.0)**$^{*\&}$	51.5 ± 9.6 (37.3, 68.6)
H-T	9.53 ± 0.96 (7.95, 11.30)	0.106 ± 0.015 (0.081, 0.135)	0.0146 ± 0.0008 (0.0132, 0.0162)	−133.6 ± 9.4 (−120.5, −153.3)	54.2 ± 9.2 (37.1, 68.5)
H-T + TTFA	9.53 ± 0.96 (7.95, 11.30)	0.106 ± 0.015 (0.081, 0.135)	0.0146 ± 0.0008 (0.0132, 0.0162)	−142.9 ± 10.2 (−130.1, −167.9)	54.2 ± 9.2 (37.1, 68.5)
H-T + Rot	**6.21 ± 0.66** **(5.35, 7.62)**$^{\&}$	**0.061 ± 0.008** **(0.049, 0.079)**$^{\&}$	**0.0059 ± 0.0004** **(0.0053, 0.0066)**$^{\&}$	**−61.8 ± 3.5** **(−55.4, −69.3)**$^{\&}$	52.9 ± 9.6 (38.4, 69.3)

Values are means ± SD of estimated values of model parameters (Monte Carlo approach) with estimated 95% confidence intervals in parentheses. For each experimental condition, the model solution was fit to the mean rhodamine 6G (R6G) data 100 times with random initial parameter values sampled from a uniform distribution within ±30% of the mean of the optimal values obtained from the normoxia group (23). Boldface highlights the experimental conditions for which the model parameters changed significantly. $\hat{k}_2$ is the apparent rate constant for R6G-B_e binding within the nonmitochondrial region, k_{2r} is the dissociation rate constant of R6G-B_e binding within the nonmitochondrial region, K_{d3} is the dissociation constant for R6G-B_m binding within the mitochondria region, P_1S_1 is the R6G permeability-surface area product across the plasma membrane, and $\Delta\psi_m$ is the mitochondrial membrane potential. H-S, susceptible to hyperoxia; H-T, tolerance to hyperoxia; Rot, rotenone; TTFA, thenoyltrifluoroacetone. *Different from corresponding normoxia group; $^{\&}$different from corresponding group with no inhibitors.

Mitochondrial Complex I–V Expressions

Results of Western blot analyses exemplified in Fig. 4*A* are shown in Fig. 4, *B* and *C*, which show the relative expression (expressed as fold change relative to the mean of the normoxia values from the same blot) of complexes I–V in lung tissue. For H-T lungs, Fig. 4*B* shows that complex I and II relative expression were 38% and 52%, respectively, lower than the corresponding relative expression in normoxia lungs. On the other hand, complex V relative expression was ∼70% higher in H-T lung tissue than normoxia.

For H-S rats, Fig. 4*C* shows that lung tissue complex I relative expression was 43% lower than in normoxia rats. There was no significant difference in the relative expressions of lung tissue complex II–V between H-S and normoxia rats.

Mitochondrial Oxygen Consumption Rates

Figure 5 shows the dynamic data (means ± SE) of buffer oxygen concentration (Fig. 5, *A–C*) and corresponding OCR (Fig. 5, *D–F*) following the addition of mitochondria isolated from lungs of normoxia, H-T, and H-S rats in the presence of pyruvate + malate (P + M, complex I substrates), glutamate + malate (G + M, complex I substrates), or succinate (Suc, complex II substrate) before (*state 2*), after the addition of ADP (*state 3*), and following the consumption of ADP (*state 4*). Additional data in the presence of succinate plus the complex I inhibitor rotenone, which are similar to those with just Suc, are not shown. The timeline of the protocol used to collect these data is shown in Fig. 1*A*. For all three groups of rats, OCR increased following the addition of ADP (*state 3*). This increase was significantly lower in H-S than normoxia

Table 3. *Injury endpoints and lung histology score*

Condition	Normoxia	H-T	H-S
Lung wet weight, g	1.37 ± 0.05 $n = 7$	1.43 ± 0.09 $n = 5$	1.34 ± 0.06 $n = 5$
Lung wet-to-dry weight ratio	5.00 ± 0.10 $n = 7$	4.89 ± 0.05 $n = 5$	5.08 ± 0.04 $n = 5$
$K_f \times 10^2$, mL/min/cmH_2O/g dry lung wt	2.30 ± 0.23 $n = 5$	1.56 ± 0.39 $n = 4$	6.36 ± 0.87$^{*\&}$ $n = 4$
Neutrophilic influx score	0 ± 0 $n = 6$	0.21 ± 0.08 $n = 4$	0.68 ± 0.05* $n = 5$
Edema score	0 ± 0 $n = 6$	0.17 ± 0.0 $n = 4$	0.55 ± 0.06* $n = 5$
Alveolar septum thickness score	0 ± 0 $n = 6$	0.38 ± 0.08 $n = 4$	0.45 ± 0.05* $n = 5$
mt-DAMPs, μg/mL	5.72 ± 0.32 $n = 6$	3.47 ± 0.04* $n = 4$	5.22 ± 0.26$^{\&}$ $n = 9$

Values are means ± SE. n = number of rats. K_f is pulmonary endothelial filtration coefficient. H-S, susceptible to hyperoxia; H-T, tolerant to hyperoxia; mt-DAMPs, mitochondrial damage-associated molecular patterns. *Different from normoxia; $^{\&}$different from H-T (one-way ANOVA with Tukey's post hoc analysis or one-way ANOVA on ranks with Dunn's post hoc analysis, $P < 0.05$).

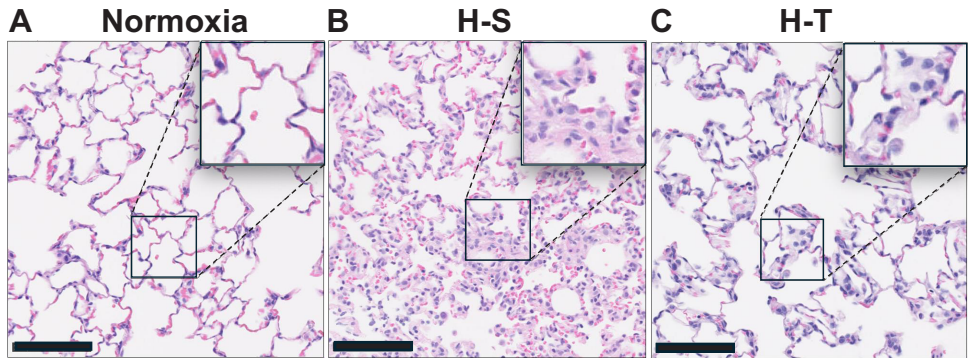

Figure 3. Images from representative rat lung slices stained with hematoxylin and eosin (H&E) from normoxia (*A*), H-S (susceptible, *B*), and H-T (tolerant, *C*) rats. Scale bar is 100 μm.

mitochondria for the different combinations of substrates studied. For H-T mitochondria, *state 3* OCR was higher than normoxia mitochondria in the presence of Suc or Suc + Rot (data not shown), but not in the presence of complex I substrates.

Figure 6 shows a summary of the substrate-specific OCRs for respiratory *states 2*, *3*, and *4* (Fig. 6, *A–C*) along with the respiratory control ratio (RCR = *state 3* OCR/*state 2* OCR; Fig. 6*D*) derived from the dynamic data in Fig. 6 as described in DATA ANALYSIS. For all three groups of rats, *state 2*, *3*, and *4* were highest in the presence of complex II substrates compared with complex I substrates, whereas RCR values were significantly lower in the presence of complex II substrate Suc in the absence (Suc) or presence (Suc + Rot) of rotenone compared with complex I substrates.

Figure 6*A* shows that for all substrate combinations, *state 2* OCRs were significantly higher in H-T mitochondria compared with those from normoxia or H-S mitochondria. There were no significant differences in *state 2* OCRs between normoxia and H-S mitochondria for the different substrate combinations studied. Figure 6*B* shows that for all substrate combinations, *state 3* OCR was significantly lower in H-S mitochondria than normoxia or H-T mitochondria. For H-T mitochondria, *state 3* OCR was not significantly different from normoxia in the presence of complex I substrates. However, *state 3* OCR was ~21% and ~19% higher in H-T mitochondria than in normoxia in the presence of complex II substrate without (Suc) or with rotenone (Suc + Rot), respectively. *State 4* OCRs (Fig. 6*C*) were also differentially altered between H-T and H-S mitochondria compared with normoxia. For H-S mitochondria, *state 4* OCR was significantly lower than normoxia in the presence of complex I substrates (~31% for P + M and ~21% for G + M), but not complex II substrate without or with rotenone. On the other hand, *state 4* OCR in H-T mitochondria was significantly higher than those in normoxia in the presence of G + M (~22%), Suc (~23%), or Suc + Rot (~28%).

Figure 6*D* shows that RCR values for H-S mitochondria were ~41%, ~30%, and ~13% lower than those for normoxia in the presence of P + M, G + M, and Suc, respectively. For H-T mitochondria, RCR values were lower than those for normoxia in the presence of P + M (~22%) and G + M (~15%), but this decrease in RCR was significantly smaller than that for H-S mitochondria compared with normoxia. There was no significant difference in the RCR between H-T and normoxia mitochondria in the presence of Suc or Suc + Rot.

For H-T mitochondria, the decrease in RCR in the presence of complex I substrates was mostly due to an increase in *state 2* OCR, whereas for H-S mitochondria, the decrease in RCR in the presence of the various combinations of substrates studied was predominantly due to a decrease in *state 3* OCR. These results suggest that H-S lung mitochondria are less coupled than lung mitochondria from H-T or normoxia rats.

We also assessed the impact of inhibiting complex I with rotenone (Rot) on mitochondrial respiration in the presence of succinate (Suc) (Fig. 6). For mitochondria from normoxia lungs, inhibiting complex I had a small (~6%) but significant effect on *state 3* OCR in the presence of Suc compared with *state 3* OCR in the presence of Suc alone. For H-S lung mitochondria, inhibiting complex I in the presence of Suc had a small but significant effect on *state 2* (−6%), *state 3* (−9%), and *state 4* (+10%) OCR compared with OCR in the presence of Suc alone.

To assess the apparent capacity of mitochondrial oxidative phosphorylation (OxPhos) and its affinity for ADP, we measured mitochondria OCR following sequentially increased ADP concentrations in the presence of complex I (P + M, G + M) or complex II (Suc) substrates (Fig. 7, *A–C*). For each ADP concentration, maximal *state 3* OCR was determined. Figure 7, *D–F*, shows a summary of the maximal *state 3* OCR as a function of ADP concentration in the presence of different substrate combinations. For all three groups, maximal *state 3* OCR in the presence of 100 μM ADP (Fig. 7, *D–F*) was significantly lower than *state 3* OCRs measured following the addition of a single ADP concentration (100 μM, Fig. 6*B*), but the decrease was larger for H-S mitochondria than for normoxia or H-T in the presence of complex I substrates. This difference between *state 3* OCRs with ADP concentration using the two different protocols is most likely due to buffer ATP accumulation and inhibition of ADP/ATP exchange (42). However, differences in *state 3* OCR among the three different groups of rats were mostly consistent using the two different protocols (Fig. 6*B* vs. Fig. 7, *D–F*). The maximal *state 3* OCR was significantly lower in H-S mitochondria compared with normoxia in the presence of complex I substrates, but not complex II substrate, for all ADP concentrations studied. For H-T mitochondria, maximal *state 3* OCR was significantly higher than corresponding values in normoxia in the presence of Suc or Suc + Rot.

To quantify the apparent affinity and capacity of mitochondrial *state 3* respiration for added ADP concentration

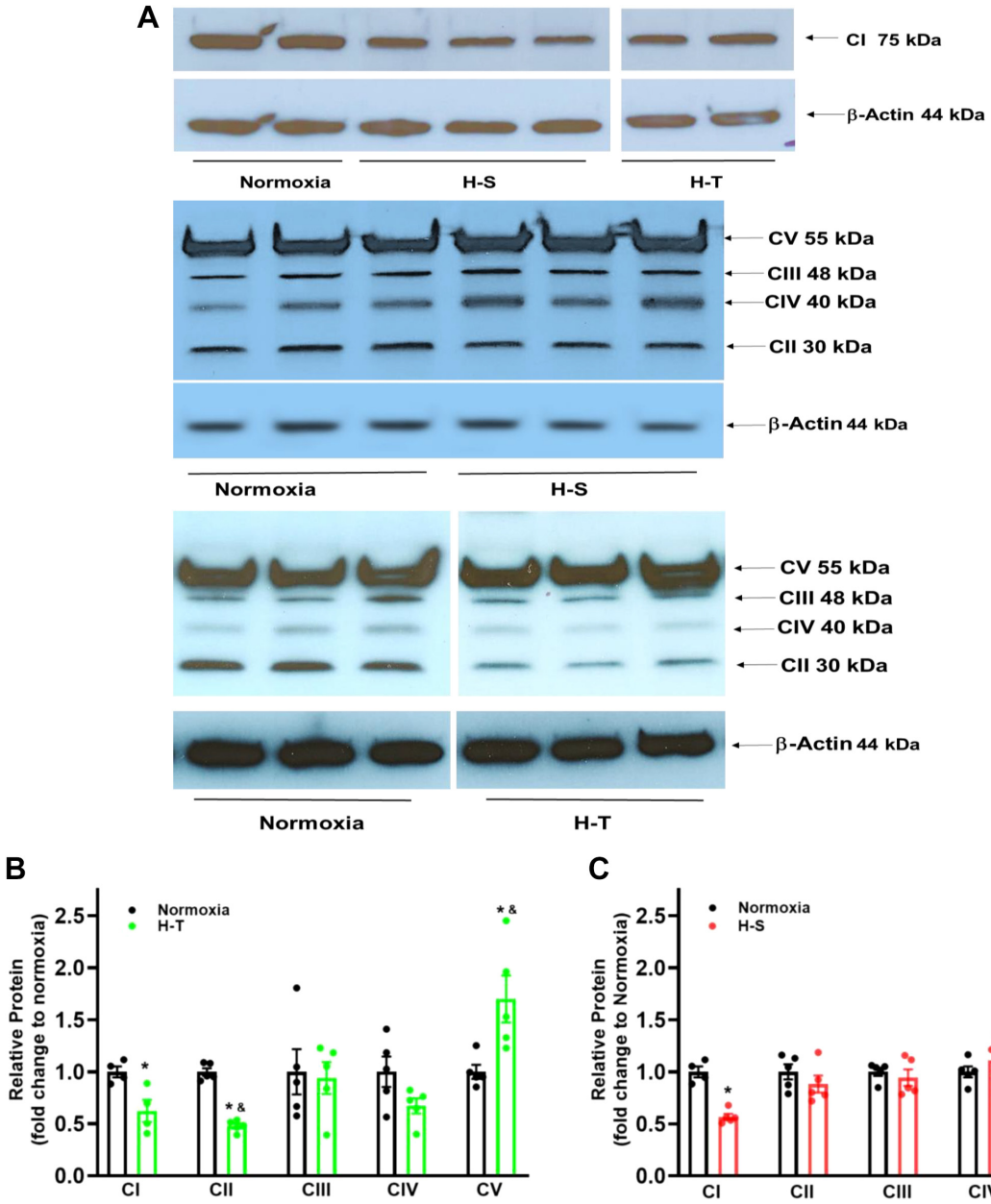

Figure 4. *A*: representative Western blots for mitochondrial electron transport chain complexes I–V (CI–CV) and corresponding β-actin that were assessed on the same gels. All spliced images were obtained from the same gel; nonpertinent lanes were removed for clarity in presentation. See Supplemental Figures S1–S5 for full Western blot images. Individual data points represent biological rather than technical replicates. For a given protein, the protein density was first normalized to the corresponding β-actin density. The normalized value is referred to as the relative protein. For each blot, relative protein values were expressed as fold change relative to mean of the normoxia values from the same blot. *B*: relative proteins of mitochondrial complexes I–V, expressed as fold change relative to mean of the normoxia values from the same blot, in lung tissue homogenates from normoxia and H-T (tolerant) rats. *C*: relative proteins of mitochondrial complexes I–V, expressed as fold change relative to mean of the normoxia values from the same blot, in lung tissue homogenate from normoxia and H-S (susceptible) rats. See Supplemental Fig. S6 for plots of protein densities and relative proteins for the different groups. Values are means ± SE. *Different from normoxia; [&]different from H-S ($n = 5$ for all groups, unpaired t test, $P < 0.05$).

([ADP]), we fit the maximal *state 3* OCR as a function of [ADP] (Fig. 7, *D–F*) to *Eq. 1*. Figure 8 provides a summary of the estimated $V_{max} + V_0$ (capacity) and K_m (affinity) of *state 3* OCR for ADP for all three groups of rats in the presence of different substrate combinations. The results show that H-S mitochondrial *state 3* OxPhos has a significantly smaller capacity (−46% for P + M and −43% for G + M), but higher affinity for ADP than normoxia mitochondria in the presence of complex I substrates. For H-T mitochondria on the other hand, *state 3* OxPhos had a higher capacity than that for normoxia mitochondria in the presence of Suc (+25%) and Suc + Rot (+26%). For H-S, inhibiting complex I decreased the affinity of *state 3* OxPhos for ADP in the presence of Suc + Rot compared with that in the presence of Suc alone. For H-T, inhibiting complex I with rotenone in the presence of Suc had a relatively small but significant effect

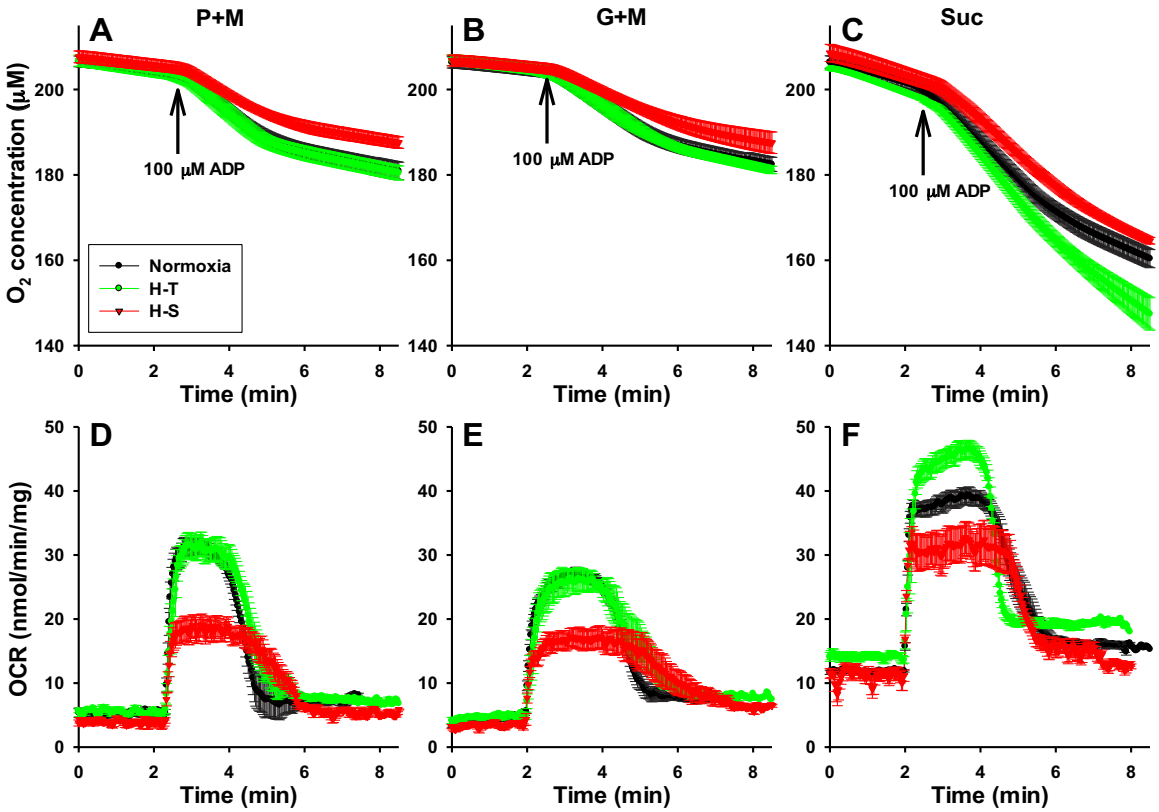

Figure 5. *A–C*: buffer oxygen (O_2) concentration reflecting aerobic metabolism following the addition of mitochondria (0.25 mg/mL) isolated from lungs of normoxia (n =11), H-T (n = 6), or H-S (n = 5) rats in the presence of complex I substrates (P + M or G + M) or complex II substrate (Suc) under *state 2*, *state 3* (addition of 100 μM ADP), and *state 4* respiration conditions. *D–F*: oxygen consumption rates (OCR) under the same experimental conditions as in *A–C*. Values are means ± SE. G + M, glutamate + malate; H-T, tolerance to hyperoxia; H-S, susceptible to hyperoxia; P + M, pyruvate + malate; Suc, succinate.

on the capacity and affinity of *state 3* OxPhos for ADP compared with those in the presence of Suc alone.

Mitochondrial Membrane Potential in Isolated Mitochondria

To assess differences in the functionality of the inner mitochondrial membrane between the three different groups of rats, we evaluated mitochondrial membrane potential ($\Delta\psi_m$) using the cationic dye TMRM.

Applying the protocol and timeline shown in Fig. 1*B*, medium TMRM emission signal (Fig. 9, *A* and *B*) was measured using our Oroboros O2K system as described in the previous section. Figure 9 shows that in the presence of P + M (complex I substrates) or Suc (complex II substrate), the addition of mitochondria stimulated a large drop in the TMRM emission signal in buffer, consistent with mitochondrial uptake of TMRM driven by $\Delta\psi_m$. The addition of ADP (*state 3*) stimulated a transient and reversible efflux of TMRM from mitochondria, consistent with transient and reversible partial depolarization of $\Delta\psi_m$. The results also show that the larger the ADP concentration, the longer it took for the TMRM to reverse back to baseline (*state 4*). Similar results were obtained with Suc (complex II substrate). We quantified the full-width half-maximum (FWHM) time for TMRM return to baseline (*state 4*) following the addition of a given ADP concentration, as a measure of the kinetics of ADP-stimulated $\Delta\psi_m$ depolarization/repolarization (24, 31). Figure 9*C* shows that in the presence of P + M, the FWHM values for H-S mitochondria were significantly longer than those for normoxia and H-T mitochondria, especially for the higher ADP concentrations (+62% for 50 μM ADP and +72% for 100 μM ADP). Figure 9*D* shows that in the presence of Suc, the FWHM values for the highest ADP concentration were differentially altered between H-S and H-T mitochondria, with the FWHM for H-S significantly longer (+21%) and the FWHM values for H-T significantly shorter (−24%) than those for normoxia.

R6G Venous Effluent Dynamic Data from Isolated Perfused Lungs

Figure 10 shows mean dynamic R6G venous effluent concentration from normoxia, H-T, and H-S lungs in the absence (Fig. 10*A*) or presence of rotenone (Fig. 10*B*) or TTFA (Fig. 10*C*). For normoxia lungs, R6G venous effluent concentration decreased from ∼0.13 μM during the loading phase to ∼0.02 μM during the washing phase, and perfusing the lungs with perfusate containing FCCP resulted in a rapid increase in the concentration of R6G in the venous effluent samples (uncoupling phase). This increase is consistent with the uncoupling of lung tissue mitochondria and the release of R6G that accumulated in the mitochondria during the loading phase, driven by $\Delta\psi_m$. The results also show no significant differences in R6G concentrations between normoxia,

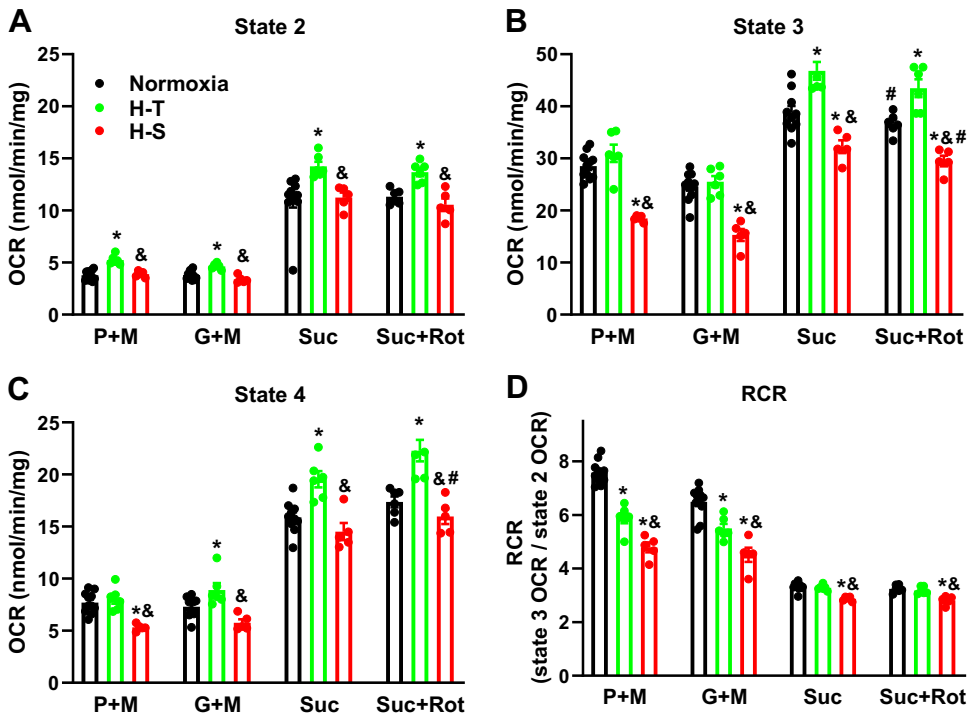

Figure 6. *State 2* (*A*), *state 3* (*B*), and *state 4* (*C*) O_2 consumption rates (OCR) along with respiratory control ratio (RCR = *state 2* OCR/*state 3* OCR) (*D*) measured in mitochondria (0.25 mg/mL) isolated from lungs of normoxia ($n = 11$), H-T (tolerant, $n = 6$), and H-S (susceptible, $n = 5$) rats in the presence of complex I substrates [pyruvate + malate (P + M) or glutamate + malate (G + M)] or complex II substrate [succinate (Suc)] without or with complex I inhibitor rotenone (Suc ± Rot) estimated from the dynamic data in the figure. *State 2* OCR was estimated as the average over a 30-s period just before the addition of ADP and *state 4* OCR was the average over a last 30 s of measurement (after steady state is reached). *State 3* OCR was estimated as the average OCR of 30-s period around the maximal OCR. Values are means ± SE. *Different from normoxia; &different from H-T (one-way ANOVA with Tukey's post hoc analysis, $P < 0.05$); #different from Suc (paired *t* test, $P < 0.05$).

H-T, and H-S lungs during the loading and washing phases. However, during the uncoupling phase, R6G peak concentration was significantly higher for H-S than for normoxia and H-T lungs. In addition, for the tail portion of the uncoupling phase, R6G concentration was significantly lower for H-T than for normoxia and H-S lungs.

To assess the role of mitochondrial complex I and II in the aforementioned observed changes, we repeated the

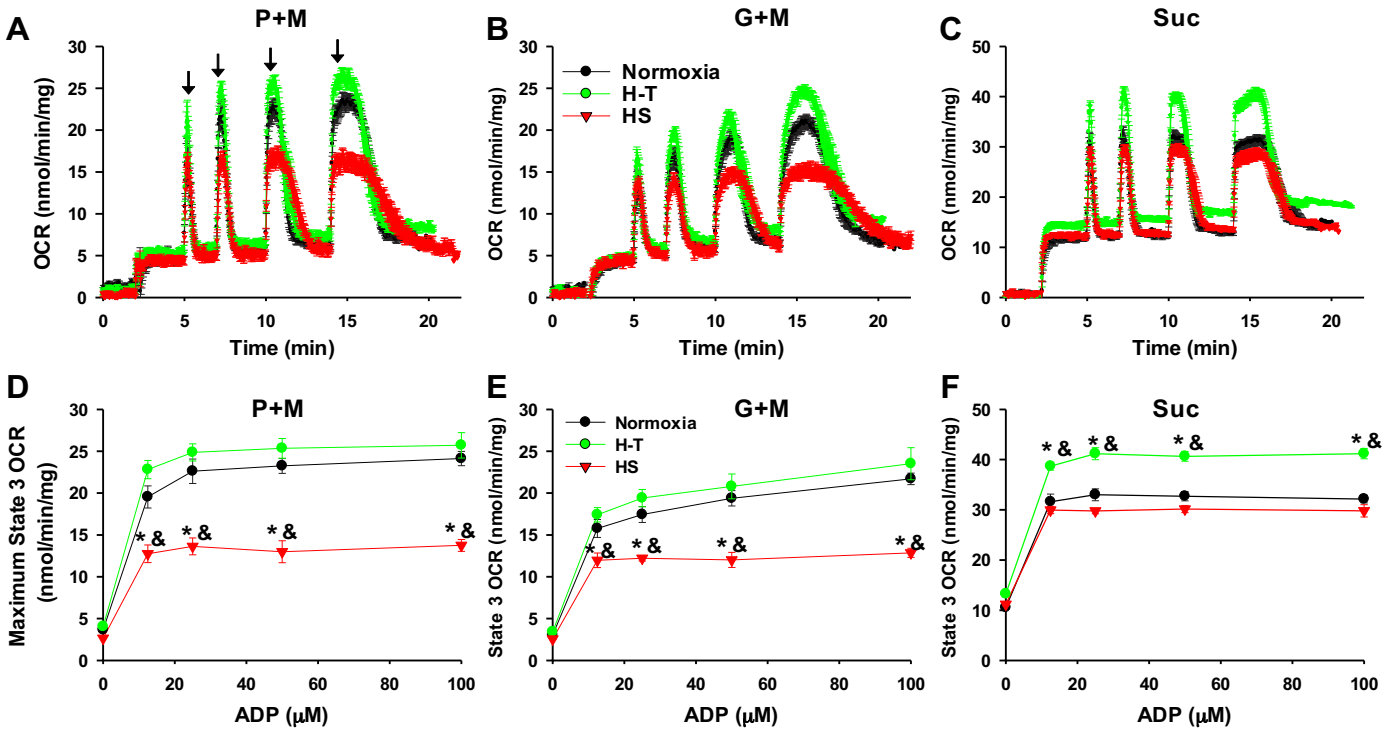

Figure 7. *A–C:* oxygen consumption rate (OCR) in mitochondria (0.25 mg/mL) isolated from the lungs of normoxia ($n = 5$), H-T (tolerant, $n = 6$), and H-S (susceptible, $n = 5$) rats in the presence of complex I substrates [pyruvate + malate (P + M) or glutamate + malate (G + M)] or complex II [succinate (Suc)] substrate in the absence or presence of rotenone (Suc + Rot, data not shown) following the sequential addition of increasing ADP concentrations (12.5, 25, 50, and 100 μM, arrows). *D–F*: maximum *state 3* OCR as a function of added ADP concentration estimated from the data in corresponding *A–C*. Values are means ± SE. *Different from normoxia; &different from H-T (one-way ANOVA with Tukey's post hoc analysis, $P < 0.05$).

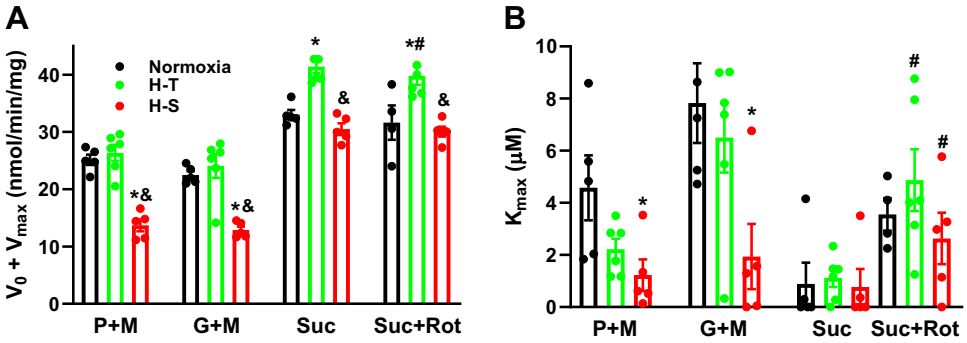

Figure 8. Estimated measures of *state 3* respiratory capacity ($V_{max} + V_0$) (*A*) and apparent affinity ($1/K_m$) (*B*) for ADP in mitochondria isolated from the lungs of normoxia ($n = 5$), H-T (tolerant, $n = 6$), and H-S (susceptible, $n = 5$) rats. V_0 is *state 2* oxygen consumption rate (OCR). For each group and substrate combination used, the values of V_{max} and K_m were estimated by fitting OCR $= V_0 + \frac{V_{max}[ADP]}{K_m + [ADP]}$ to the OCR vs. ADP concentration, [ADP], data in Fig. 7, *D–F*. Values are means ± SE. *Different from normoxia; &different from H-T (one-way ANOVA with Tukey's post hoc analysis, $P < 0.05$); #different from succinate (Suc) (paired *t* test, $P < 0.05$). G + M, glutamate + malate; P + M, pyruvate + malate; Rot, rotenone.

experimental protocol in Fig. 10*A* in the presence of either rotenone (complex I inhibitor) or thenoyltrifluoroacetone (TTFA, complex II inhibitor).

Effect of Inhibiting Complex I with Rotenone on R6G Venous Effluent Dynamic Data

Figure 10*B* and Fig. 11 show that for all three groups of lungs, inhibiting complex I with rotenone increased R6G venous effluent concentration during the loading and washing phases but decreased R6G concentration during the uncoupling phase, compared with R6G concentration in the absence of rotenone. These changes are consistent with rotenone-induced $\Delta\psi_m$ depolarization and with a dominant role for complex I in $\Delta\psi_m$. However, the increase in R6G venous effluent concentration during the loading phase was significantly lower in H-S lungs than in normoxia lungs (Fig. 10*B*). This could be due to the decrease in mitochondrial complex I activity/expression in H-S lungs or a difference in the effect of rotenone on R6G binding in the cytoplasm and/or mitochondrial regions (see DISCUSSION). Furthermore, Fig. 10*B* shows that for the uncoupling phase, R6G concentration for H-T lungs was significantly lower than H-S. This may suggest a larger contribution from complex I to $\Delta\psi_m$ in H-T than in H-S lungs (see DISCUSSION).

Effect of Inhibiting Complex II with TTFA on R6G Venous Effluent Dynamic Data

Figure 10*C* shows that R6G concentrations during all three phases were not different between the three groups. For normoxia lungs, Fig. 11*A* shows that inhibiting complex II with

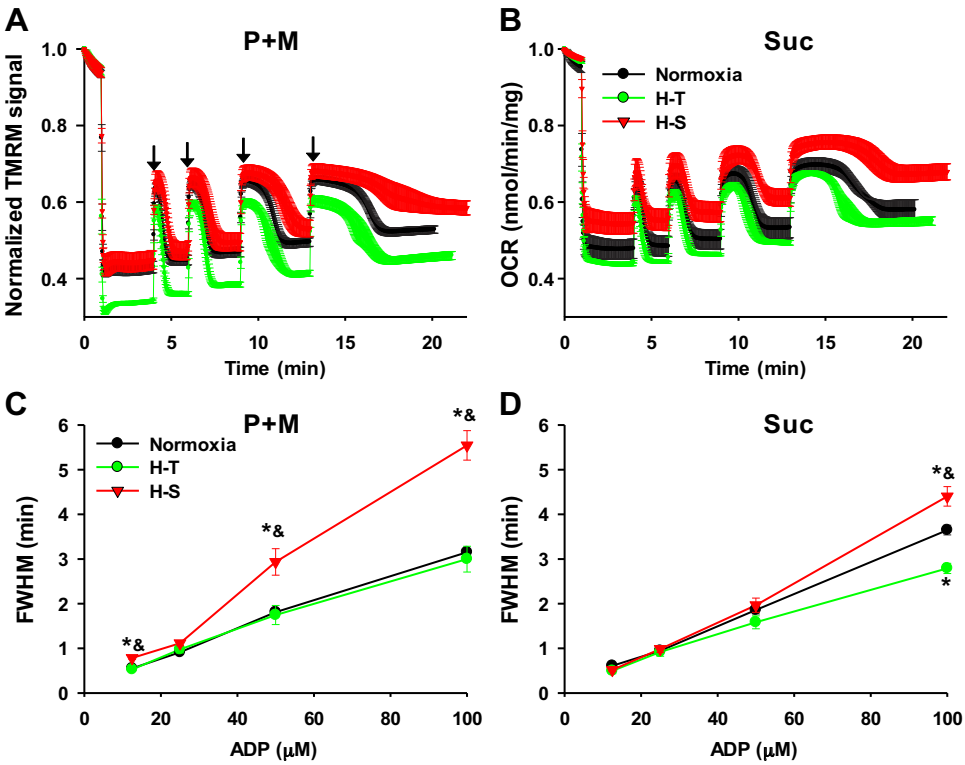

Figure 9. *A* and *B:* averaged tetramethylrhodamine methyl ester (TMRM) emission signal in mitochondria isolated from the lungs of normoxia ($n = 4$), H-T (tolerant, $n = 4$), and H-S (susceptible, $n = 4$) rats in the presence of complex I substrates [pyruvate + malate (P + M)] or complex II substrate [succinate (Suc)] following the sequential addition of increasing ADP concentrations. *C* and *D:* we quantified the full-width half-maximum time (FWHM) for TMRM return to baseline (*state 4*) following the addition of a given ADP concentration, as a measure of the kinetics of ADP-stimulated $\Delta\psi_m$ depolarization/repolarization. Values are means ± SE. *Different from normoxia; &different from H-T for the same ADP concentration (one-way ANOVA with Tukey's post hoc analysis, $P < 0.05$).

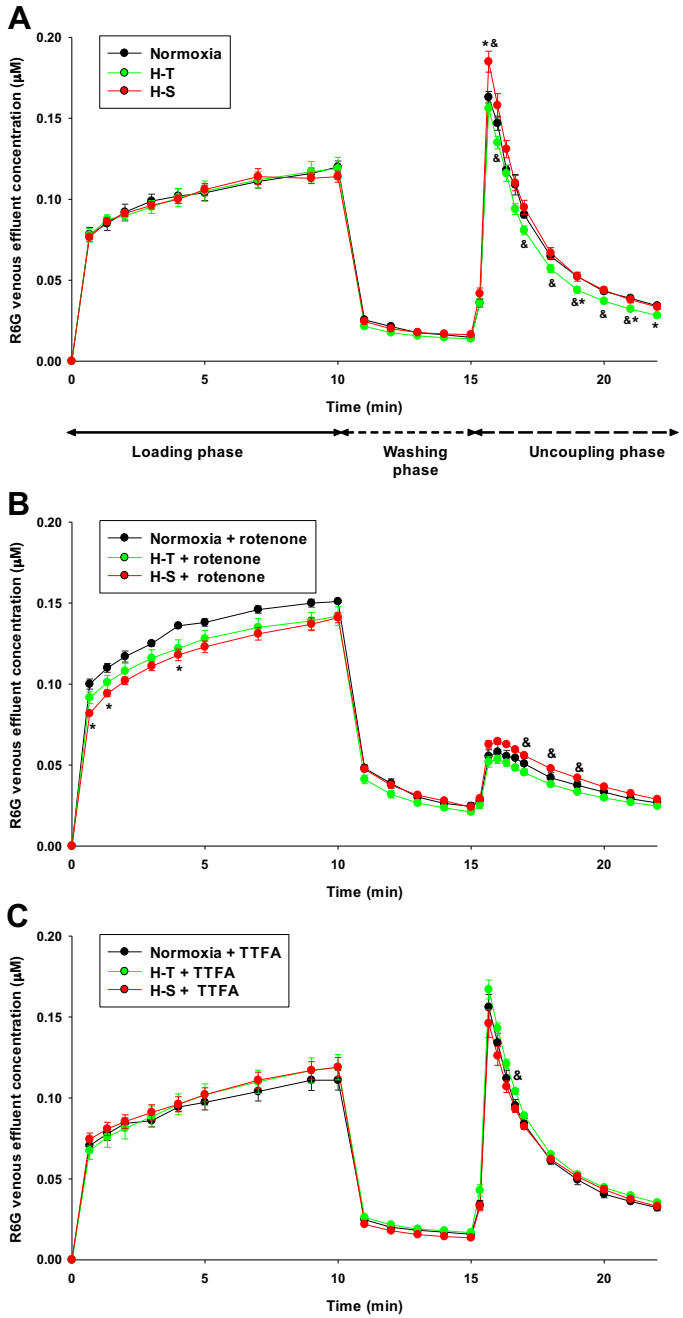

Figure 10. *A:* Rhodamine 6G (R6G) venous effluent concentration in normoxia (black, $n = 5$), H-T (tolerant, green, $n = 5$), and H-S (susceptible, red, $n = 4$) rat lungs during the three phases of the experimental protocol. *B:* R6G venous effluent concentration in normoxia (black, $n = 4$), H-T (green, $n = 5$), and H-S (red, $n = 3$) rat lungs during the three phases of the experimental protocol in the presence of rotenone (complex I inhibitor). *C:* R6G venous effluent concentration in normoxia (black, $n = 4$), H-T (green, $n = 5$), and H-S (red, $n = 4$) rat lungs during the three phases of the experimental protocol in the presence of thenoyltrifluoroacetone (TTFA) (complex II inhibitor). Values are means ± SE. *Different from normoxia; &different from H-S (one-way ANOVA with Tukey's post hoc analysis, $P < 0.05$).

TTFA had no significant effect on R6G concentration during all three phases, which suggests that complex II does not contribute much to $\Delta\psi_m$ in normoxia lungs. For H-T lungs (Fig. 11*B*), there was no significant effect on R6G concentration during the loading and washing phases; however, R6G concentration during the tail end of the uncoupling phase tended to be higher in the presence versus absence of TTFA. For H-S lungs (Fig. 11*C*), TFFA had no significant effect on R6G concentration during the loading and washing phase. However, R6G concentration was significantly lower during the uncoupling phase compared with the concentration in the absence of TTFA, suggesting a potential contribution from complex II to $\Delta\psi_m$ in H-S lungs.

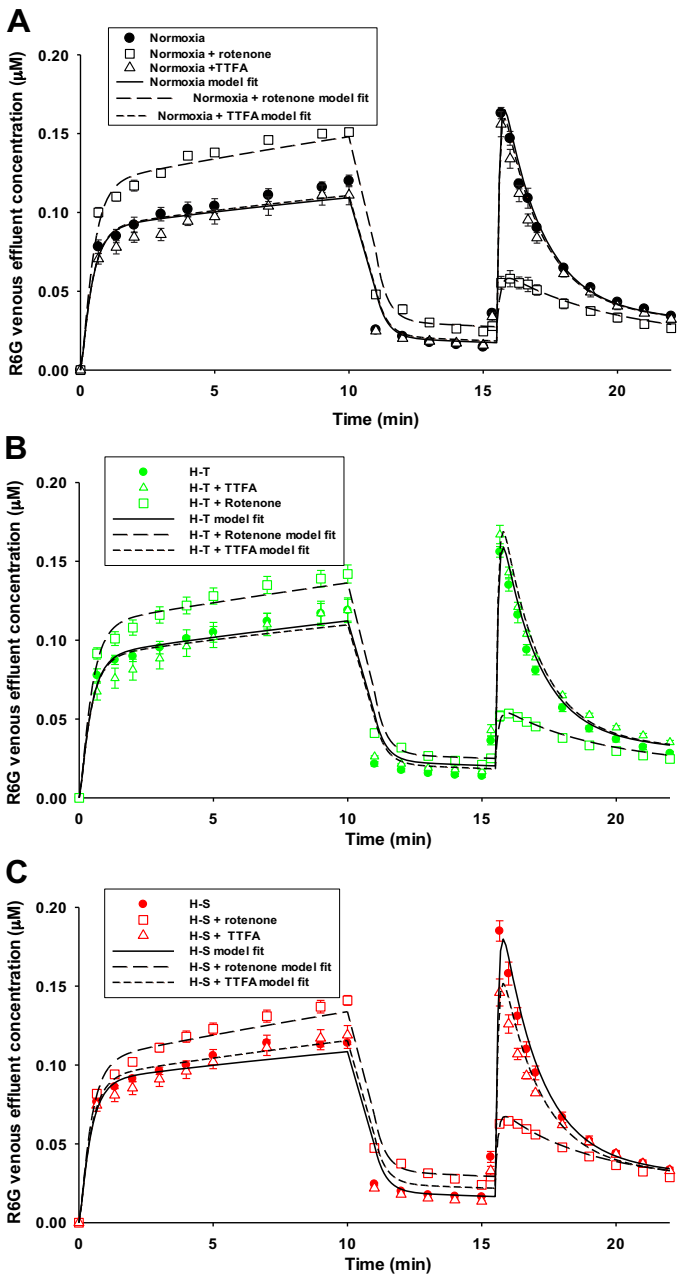

Figure 11. Rhodamine 6G (R6G) venous effluent concentration from the lungs of normoxia (*A*), H-T (tolerant, *B*), and H-S (susceptible, *C*) rats in the absence ($n = 5$, 4, and 5) or in the presence of rotenone ($n = 4$, 5, 3) or thenoyltrifluoroacetone (TTFA) ($n = 4$, 5, and 5) during the three phases of the experimental protocol. Dashed lines superimposed over the data in *A–C* are the fits of a physiologically based pharmacokinetic model of R6G disposition on the passage through the pulmonary circulation. Values are means ± SE.

Table 4. *Summary of the effect of rat exposure to H-S or H-T on cellular processes and lung uptake of SPECT biomarkers*

	H-S % Change from Normoxia	References	H-T% Change from Normoxia	References
Complex I activity	−51%	(25)	−49%	(24)
Complex II activity	NA		NS	(24)
Complex III activity	NS	(25)	NA	
Complex IV activity	−25%	(26)	39%	(24)
Complex I expression	−43%	Present study	−38%	Present study
Complex II expression	NS	Present study	−52%	Present study
Complex III expression	NS	Present study	NA	Present study
Complex IV expression	NS	Present study	NA	Present study
Complex V expression	NS	Present study	+70%	Present study
RCR (complex I substrates, P + M)	−41%	Present study	−22%	Present study
RCR (complex II substrate, Suc)	−13%	Present study	NS	Present study
State 2 OCR (P + M)	NS	Present study	+39%	Present study
State 2 OCR (Suc)	NS	Present study	+22%	Present study
State 3 OCR (P + M)	−35%	Present study	NS	Present study
State 3 OCR (Suc)	−17%	Present study	+21%	Present study
FWHM (P + M)	+72%	Present study	NS	Present study
FWHM (Suc)	+ 21%	Present study	−24%	Present study
$K_f \times 10^2$, mL/min/cmH_2O/g dry lung wt	+177%	Present study	NS	(24)
GSH content	+19%	(26)	+40%	(26)
GSH synthetase expression	NA		+44%	(24)
G-6-PDH per g dry wt	NS	(25)	NA	
g-Glutamyl transferase per μU/mg	NS	(25)	NA	

FWHM, full-width half-maximum, a measure of the kinetics of ADP-stimulated mitochondrial membrane potential ($\Delta\psi_m$) depolarization/repolarization (100 μM ADP concentration); G-6-PDH, glucose 6 phosphate dehydrogenase; GSH, glutathione; H-S, susceptible to hyperoxia; H-T, tolerance to hyperoxia; K_f, pulmonary endothelial filtration coefficient; NA, not available; NS, not significant; P + M, pryruvate + malate; Suc, succinate.

Computational Modeling Results

Figure 11 shows model fits to mean data from normoxia, H-T, and H-S lungs in the absence or presence of either rotenone or TTFA. The model parameter values estimated by simultaneously fitting R6G data without and with TTFA were not different for K_{d3}, $\hat{k}_2$, k_{2r}, and P_1S_1 among the three groups of lungs based on the significant overlap of the confidence intervals for a given parameter. For normoxia lungs, estimated values of $\Delta\psi_m$ (Table 2) with and without TTFA were not significantly different. For H-S lungs, the estimated value of $\Delta\psi_m$ depolarized from −149.7 mV in the absence of TTFA to −124 mV in the presence of TTFA, but this difference was not statistically significant based on the confidence intervals (Table 2). The tendency of $\Delta\psi_m$ in H-S lungs to be more depolarized, although not statistically significant, in the presence compared with that in the absence of TTFA is consistent with a contribution of complex II to $\Delta\psi_m$. For H-T lungs, $\Delta\psi_m$ tended to be more hyperpolarized in the presence (−143 mV) than in the absence (−134 mV) of TTFA, but again the difference was not statistically significant due to overlapping confidence intervals.

As expected, inhibition of complex I activity with rotenone significantly depolarized $\Delta\psi_m$ from −147 mV to − 57 mV for normoxia lungs, from −149 mV to −72 mV for H-S lungs, and from −134 mV to −62 mV for H-T lungs (Table 2). The estimated value of $\Delta\psi_m$ in the presence of rotenone was significantly higher (more hyperpolarized) in H-S lungs than in normoxia lungs. The rotenone-induced drop in $\Delta\psi_m$, as a percentage of $\Delta\psi_m$ in the absence of rotenone, was 61% for normoxia versus just 52% in H-S lungs. These observations are consistent with a smaller contribution from complex I to $\Delta\psi_m$ in H-S lungs than in normoxia or H-T lungs.

For normoxia and H-T lungs, the addition of rotenone significantly decreased the values of $\hat{k}_2$, k_{2r}, and K_{d3}, but had no effect on the value of P_1S_1 (Table 2) (23). For H-S lungs, rotenone significantly decreased K_{d3} but had no significant effect on the other parameters. The value of $\hat{k}_2$ in the presence of rotenone was significantly higher for H-S than normoxia lungs. This could be due to the effect of rotenone on R6G binding kinetics within the nonmitochondrial and mitochondrial regions based on changes in the redox states within these regions resulting from the partial depolarization of $\Delta\psi_m$, as discussed by Audi et al. (23).

DISCUSSION

The objective of this study was to test the hypothesis that lung mitochondrial processes are differentially altered between H-S and H-T rats compared with control (normoxia) rats by evaluating lung tissue mitochondrial bioenergetics, since currently little is known (13, 14, 24–26). Our results demonstrate differences in the mitochondrial bioenergetics of H-T and H-S lungs measured at different levels of biological organization. Furthermore, our data show that although rat exposure to 60% O_2 for 7 days had no apparent effect on overall rat health, as measured by body weight gain, it did cause lung injury as measured by mitochondrial bioenergetics, histology by light microscopy, and pulmonary vascular endothelial filtration coefficient (K_f). The contribution of such changes to the observed tolerance of H-T and susceptibility of H-S rats is an important question but depends first on the results presented in the current study.

Western Blot Studies

Previously, we measured the activity of complex I, II, III, and/or IV in the lung tissue homogenate from H-S and H-T

rats (Table 4) (24–26). The measured decreases in complex I expression in the present study (Fig. 4) are consistent with the previously measured decreases in complex I activity in H-T (49%) and H-S (51%) lung tissue homogenate (24–26). However, it is not clear whether this decrease in lung tissue complex I expression/activity has a significant impact on lung tissue mitochondrial function since complex I is normally in excess (24, 43). A previous study showed that a reduction of up to 40% of complex I activity has only a modest effect on cell respiration in various cell types (43).

Previously, we reported that complex II activity in the lung tissue homogenate from H-T rats was not significantly different from that of normoxia rats (Table 4) (24). This is consistent with the measured OCR and RCR in isolated mitochondria from H-T lungs in the presence of complex II substrate succinate (Fig. 6). However, Fig. 4*B* shows a 52% decrease in the expression of complex II in H-T lung compared with that of normoxia lungs. Although a Western blot detects the primary structure of an expressed protein, activity depends on, among other factors, the correct folding of the enzyme, the presence of co-factors, proper subcellular targeting, or mutations of crucial catalytic residues. Other factors that could affect complex II activity, but not expression, include the contribution of the targeted subunit (with the chosen antibody) to complex II activity, changes in substrate availability, and regulatory molecules that may have changed to counter the decrease in complex II expression and preserve complex II activity. Regardless, as discussed under $\Delta\psi_m$ *in Isolated Perfused Lungs*, complex II appears to provide only a minor contribution to the pulmonary mitochondrial electron transport chain (ETC) in intact rat lungs.

The results from the present study show no significant change in lung tissue complex IV expression with H-T, but a 70% increase in complex V expression (Fig. 4). The lack of change in complex IV expression should be interpreted in the context of our results from a previous study in which we reported ∼40% increase in the activity of complex IV in H-T lung tissue homogenate (Table 4) (24, 26). The increase in lung complex V expression and the previously measured increase in complex IV activity in H-T rats could be a means of decreasing reactive oxygen species (ROS) production at complexes I, II, and III, since the higher the respiration rate, the less time the electrons are delayed at critical leakage sites (such as complex I, II, and III) by depleting upstream electron-rich intermediates such as ubisemiquinone that lead to ROS formation (25, 44, 45). This interpretation would be consistent with the measured 40% decrease in mt-DAMPs plasma concentration in H-T rats compared with normoxia rats. Mitochondrial oxidative stress leads to mitochondrial damage and release of mt-DAMPs, including damaged mtDNA, into the cytosol and plasma region, where they can stimulate an inflammatory response and an increase in endothelial permeability (46, 47). Thus, changes in the activity of ETC complexes, especially the increase in complex IV activity and complex V expression with normal mitochondrial membrane potential (see $\Delta\psi_m$ *in Isolated Perfused Lungs*) may be an important factor in the tolerance of H-T rats to hyperoxia. Additional studies would be needed to evaluate the effect of these changes on lung mitochondrial ROS formation.

Isolated Mitochondria OCR Studies

For the isolated mitochondria studies, the integrity of mitochondria was based on the respiratory control ratio (RCR) in the presence of P + M, which for the present study was ∼7.6 for normoxia rats. This number is higher than previously reported RCR for mitochondria isolated from normoxia rat lung tissue, perhaps reflecting optimization of our isolation techniques (39, 42, 48–52).

To assess the stability of our isolated mitochondria preparation while kept on ice, we measured RCR in isolated mitochondria from the lungs of a normoxia rat in the presence of pyruvate + malate at *time 0* (∼15 min after isolation) and 2 h later. RCR was initially 7.34 and then 7.69 at 2 h, consistent with the stability of our isolated mitochondria preparation over a period of at least 2 h.

State 2 OCR was significantly higher for H-T than for normoxia mitochondria for all combinations of substrates (Fig. 6*A*). *State 2* is the mitochondrial respiration state in the absence of ATP synthesis, presumably due to proton leak through the inner mitochondrial membrane (53). This proton leak dissipates the protonmotive force (Δp) due to the reentry of H^+ into the mitochondrial matrix in the absence of ATP synthesis. Thus, our data support a lack of complete coupling between respiration and phosphorylation in H-T rats. Mechanisms involved in uncoupling of mitochondria and hence H^+ leak include uncoupling proteins, the adenine nucleotide translocase (ANT), and the mitochondrial permeability transition pore (MPTP) (53). Under normal conditions, *state 2* proton leak is predominantly via uncoupling proteins and increases nonlinearly with an increase in Δp, which consists of electrical ($\Delta\psi_m$) and chemical (ΔpH) components. A relatively small increase in leak (mild uncoupling) slightly lowers Δp, which may decrease mitochondrial ROS generation and minimize oxidative stress without a significant effect on ATP synthesis (54). As such, an increase in *state 2* OCR may be protective (so called "uncoupling to survive" hypothesis) during hyperoxia (54), especially when it is concomitant with a proportional increase in *state 3* OCR, which is the case for H-T mitochondria (Fig. 6*B*). A relatively high Δp leads to a more reduced ETC and a decrease in the flow of electrons through the chain, resulting in an increase in the leak of electrons that react with O_2 to generate superoxide (53). Measuring ROS production in isolated mitochondria would be needed to assess the impact of this increase in *state 2* OCR on mitochondrial ROS generation in H-T mitochondria but is beyond the scope of this work.

State 3 OCR measured using the single ADP concentration protocol (Fig. 1*A*) was significantly lower in H-S mitochondria than in normoxia and H-T for both complex I and II substrates (Fig. 6*B*). For H-T mitochondria, *state 3* OCR in the presence of Suc was significantly higher (∼21%) than normoxia. *State 3* OxPhos capacity for ATP synthesis (V_{max}) estimated from the data in Fig. 7, *D–F* was differentially altered between H-T and H-S mitochondria (Fig. 8). For H-S, V_{max} decreased by ∼46% and ∼43% in the presence of P + M and G + M, respectively (Fig. 8*A*). In contrast, for H-T, V_{max} increased by ∼16% and ∼25% in the presence of G + M and Suc, respectively (Fig. 8*A*). For H-S, the affinity of *state 3* OCR for ADP (inverse of K_m) increased in the presence of complex I substrates (Fig. 8*B*). The increase in V_{max} for H-T

mitochondria is consistent with the increase in the expression of complex V measured in the present study (Fig. 4) and in the activity of complex IV (Table 4) previously measured (24, 26). For H-S, the decrease in V_{max} in the presence of complex I substrates could be due to the decrease in complex I activity/expression (Fig. 4 and Table 4) or decrease in complex IV activity previously reported (Table 4) (26).

Results in Fig. 6*D* indicate that for H-S mitochondria, RCR values were ~41%, ~30%, and ~13% lower than normoxia mitochondria in the presence of P + M, G + M, and Suc, respectively. For H-T, RCR was only ~22% and ~15% lower than normoxia in the presence of P + M and G + M, respectively. RCR for H-T and normoxia mitochondria was not different in the presence of succinate. These results suggest that H-S mitochondria are significantly more uncoupled than H-T or normoxia mitochondria.

For all groups of rats, *state 4* OCR was higher than *state 2* OCR for all substrate combinations (Fig. 6*C*). *State 4* respiration reflects not only intrinsic proton leak (*state 2*) but also ATP hydrolysis activity due to recycling of some ATP back to ADP due to high ATP/ADP ratio (42). Carlson et al. (42) showed adding ATP to the mitochondria respiration buffer, which increases matrix ATP via reverse adenine nucleotide translocator (ANT), increases respiration of mitochondria isolated from rat lung tissue. Furthermore, they showed that inhibiting ANT eliminated the difference between *state 2* and *state 4* OCR and the ATP-stimulated increase in OCR (42). For H-T mitochondria, the higher *state 4* OCR, compared with normoxia, is mostly due to higher *state 2* OCR (Fig. 6).

Reversed electron transport (RET) occurs when NAD^+ is reduced to NADH via the transfer of electrons from ubiquinol to complex I (55). This mechanism, first reported by Chance and Hollunger (56) when they observed the reduction of NAD^+ to NADH in isolated mitochondria in the presence of succinate (Suc), is an important source of mitochondrial ROS. One approach to detect and quantify RET in isolated mitochondria is to measure OCR in the presence of Suc, without (Suc) and with (Suc + Rot) the complex I inhibitor rotenone. An increase in *state 3* OCR with Suc + Rot compared with OCR with Suc only is indicative of RET. For normoxia mitochondria, inhibiting complex I had no significant effect on mitochondria respiration, including *state 3* OxPhos capacity for ATP synthesis or the affinity of *state 3* for ADP (Fig. 8). For H-S mitochondria, inhibiting complex I decreased the affinity of *state 3* OxPhos for ADP with Suc + Rot as compared with Suc alone. For H-T, using Suc + Rot had a small but significant effect on the capacity and affinity of *state 3* OxPhos for ADP compared with Suc alone (Fig. 8). Overall, for all three groups of mitochondria inhibiting complex I had a relatively small effect on *state 3* OCR in the presence of Suc. These results suggest efficient conversion of ADP to ATP in rat lung mitochondria in the presence of Suc, and that RET is not an important mechanism in lung mitochondrial bioenergetics in any of the three rat groups. Similar results were reported by Carlson et al. (42) in mitochondria from control rats.

Hayatdavoudi et al. (14) reported no significant difference in the O_2 consumption rate of lung tissue slices from normoxia and H-S rats in the absence or presence of a mitochondrial uncoupler. Based on these results, they concluded that overall tissue mitochondrial function was not significantly altered in H-S lungs (14). The approach they used to measure O_2 consumption is sensitive to many factors, including slice thickness, incubation conditions, buffer used, temperature, head space gas, and shaking frequency (57).

Mitochondrial Membrane Potential in Isolated Mitochondria

To assess the effect of H-T and H-S on $\Delta\psi_m$ in isolated mitochondria, we evaluated the kinetics of mitochondrial uptake of the cationic compound TMRM. The results show that FWHM values for H-S mitochondria in the presence of P + M were significantly longer (+85%) than normoxia or H-T, especially for the higher ADP concentrations. This is consistent with a lower capacity of *state 3* for ADP and a decrease in complex I activity/expression. These results suggest that $\Delta\psi_m$ is partially depolarized in H-S mitochondria. For H-T mitochondria, the results suggest that the ~70% increase in complex V expression and previously reported increase in complex IV activity were sufficient to counter the potential effect of a decrease in complex I expression/activity on $\Delta\psi_m$, and hence preserve $\Delta\psi_m$. In the presence of Suc, FWHM values at the highest ADP concentration were differentially altered between H-S (+21%) and H-T (−24%), consistent with changes in *state 3* capacity for ADP in the presence of Suc. This suggests a slight increase in $\Delta\psi_m$ (hyperpolarized) in H-T mitochondria potentially due to increased complex IV activity and complex V expression with no change in complex II activity (Table 4). For H-S, we observed a slightly depolarized $\Delta\psi_m$ in the presence of succinate despite no change in complex II–V expression. It is possible that the activity of complex II or other complexes decreased with no change in expression. Previously, we reported a decrease (25%) in complex IV activity in H-S lung tissue homogenate (Table 4) (26), which could contribute to the partial depolarization of $\Delta\psi_m$.

$\Delta\psi_m$ in Isolated Perfused Lungs

Computational modeling of the R6G venous effluent concentration data reveals no significant difference in $\Delta\psi_m$ in isolated perfused lungs from the three groups of rats. Therefore, changes in mitochondrial processes measured in isolated mitochondria from lungs of H-S and H-T rats could be countered by other adaptive shifts (i.e., availability of substrates, regulation molecules, etc.) to preserve lung tissue $\Delta\psi_m$ under normoxia conditions.

Computational modeling analysis (Table 2) of the R6G venous effluent concentration from isolated perfused normoxia lungs show that inhibiting complex I had a large effect on $\Delta\psi_m$, depolarizing it from −147 mV to −57 mV, whereas inhibiting complex II had no significant effect on $\Delta\psi_m$. These data suggest that complex I is the dominant source of electrons flowing through ETC, with essentially no contribution from complex II. This interpretation is consistent with data by Bongard et al. (22), which showed that inhibiting complex I decreased lung tissue total maximum ATP content by about the same fraction (−80%) as inhibiting complex III (−78%), which is equivalent to inhibiting both complex I and II. Mitochondrial respiration accounts for 80–

85% of total lung ATP content (80–85%) (22, 58). The concentration of TTFA used in the present study is similar to that used in previous studies in isolated perfused rat lungs (59, 60). Previously, we showed that this TTFA concentration inhibited ~76% of the H_2O_2 released by isolated perfused lungs, suggesting that complex II is the dominant source of ROS in lung tissue mitochondria (59). These results imply that in normal rat lungs, complex I is the dominant source of electrons for the ETC, whereas complex II is the dominant source of ROS.

Additional computational modeling of the R6G data from H-T lungs show similar results as those from normoxia lungs in terms of estimated $\Delta\psi_m$ and the contributions of complex I and complex II to $\Delta\psi_m$. However, for H-S lungs, modeling results show that the estimated value of $\Delta\psi_m$ in the presence of rotenone was significantly larger (more hyperpolarized, −72 mV) than normoxia (−57 mV) and that the rotenone-induced drop in $\Delta\psi_m$, as a percentage of $\Delta\psi_m$ in the absence of rotenone, was larger in normoxia (61%) than H-S (52%) lungs. Furthermore, $\Delta\psi_m$ for H-S lungs tended to be more depolarized in the presence of TTFA (−124 mV) than in its absence (−150 mV), although the difference was not statistically significant (Table 2). These results suggest that complex II makes a larger contribution to the mitochondria ETC in H-S than in normoxia or H-T lungs, consistent with a partial shift in tissue mitochondrial bioenergetics in H-S lungs from complex I to complex II.

In the isolated mitochondria studies, the complex II substrate Suc was capable of energizing the mitochondria as reflected by OCR and TMRM data, whereas in intact lungs complex II makes virtually no contribution to the mitochondrial ETC. To understand this apparent difference between isolated mitochondria and mitochondria in intact lungs, complex II function is considered.

Complex II consists of four subunits namely a flavoprotein (SDHI), an iron-sulfur subunit (SDH2), and two member subunits (SDH3 and SDH4), all encoded by nuclear DNA (61). Unlike complexes I, III, and IV, complex II is not a proton pump. Instead it oxidizes succinate to fumarate (succinate dehydrogenase activity) in the Krebs cycle and in the process provides two electrons to ETC by reducing ubiquinone. Thus, complex II is unique in that it is the only enzyme that is a component of both the ETC and the Krebs cycle, thus linking these two vital mitochondrial processes. The oxidation of succinate to fumarate (succinate dehydrogenase activity) is countered by the conversion of fumarate to succinate (fumarate reductase activity). In the isolated mitochondria studies, fumarate reductase activity is inhibited by the addition of a large concentration of exogenous succinate, which maximizes the succinate dehydrogenase activity of complex II. It is possible that in intact lungs, fumarate reductase activity is high enough to counter succinate dehydrogenase activity such that complex II makes only a minor contribution to the mitochondrial ETC. This could explain the differences between the results from isolated mitochondria and isolated perfused lungs as far as the contribution of complex II to ETC. This balance between succinate dehydrogenase activity and fumarate activity of complex II may have changed in H-S lungs, resulting in a larger contribution of complex II to the ETC than in normoxia or H-T lungs.

A previous study showed succinate dehydrogenase activity is relatively low in pulmonary arterial walls, and high in bronchiolar epithelial cells (62). As such, one limitation of the use of R6G to probe tissue $\Delta\psi_m$ in isolated perfused lungs is that the venous concentration of R6G is affected predominantly by pulmonary endothelial cells since these cells are in direct contact with the perfusate and account for ~50% of the lung cells, whereas mitochondria isolated from lung tissue contain mitochondria from all lung cells, including epithelial cells.

Lung Vascular Endothelial Filtration Coefficient

Previously, Bongard et al. (22) established a connection between mitochondrial dysfunction and pulmonary vascular permeability as measured by K_f. The change in mitochondrial bioenergetics in lung tissue of H-S rats measured in the present study could account for the measured 177% increase in K_f in H-S lungs.

Hayatdavoudi et al. (14) reported no difference between the lung wet or wet/dry wet ratios of normoxia and H-S rats in the absence of mechanical ventilation or perfusion. However, when the rats were exposed to high positive ventilation pressure for 30 min, lung wet and wet/dry ratios of H-S rats increased by fourfold compared with just 50% in normoxia rats (14). This is consistent with the results of the present study, which show that wet and wet/dry ratios of unperfused lungs from H-S rats were not different from normoxia, but K_f, whose measurement requires exposure of lungs to high perfusion pressures, was significantly higher in lungs of H-S rats compared with that in lungs of normoxia rats (Table 3).

Previously, we reported that rat exposure to >95% O_2 for 48 h increased K_f by 213%, decreased complex I (78%) and complex II (66%) activity, increased complex IV activity (47%), and partially depolarized lung tissue $\Delta\psi_m$ (from −140 mV to −107 mV), and that subsequent exposure to room air for 24 h (H-T rats) partially reversed the decrease in complex I activity, fully reversed the decrease in complex II activity, maintained the increase in complex IV activity, and fully reversed the increase in K_f (24). Results from the present study show that subsequent exposure to room air for 24 h (H-T) fully reversed the depolarization in lung tissue $\Delta\psi_m$. These mitochondrial changes could account for the reversal of the increase in K_f after 48 h of exposure to >95 O_2 (24).

Limitations

Published data regarding the rat models of tolerance (H-T) and susceptibility (H-S) to hyperoxia have come from studies that used only male rats (13, 14). Since the time- or dose-response necessary to develop tolerance and/or susceptibility to hyperoxia is not known in female rats, male rats were used in the present studies. We plan to carry out similar studies in female rats in the future once we confirm that tolerance and susceptibility to hyperoxia can be induced in female rats.

Potential Mechanisms of the Protection from Hyperoxia-Induced Injury in H-T Rats

There is ample evidence that oxidative stress and mitochondrial dysfunction play a key role in the pathogenesis of hyperoxia-induced ARDS (16–19, 22, 63, 64). Hyperoxia-

induced increases in reactive oxygen species (ROS) formation can overwhelm antioxidants that cannot respond quickly enough to prevent cellular oxidant injury including denaturing of proteins, oxidation of membrane lipids, and damage to nuclear and mitochondrial DNA. H-T tolerance of and H-S susceptibility to hyperoxia-induced oxidative stress could involve a change in lung tissue antioxidant content to counter increased ROS formation that leads to oxidative stress and mitochondrial dysfunction, a change in the response of cellular antioxidant systems to increased ROS formation, a change in the rate of ROS formation under hyperoxic conditions, a change in pro- or antiapoptotic mechanisms, or a combination thereof (24, 44).

Hayatdavoudi et al. (14) suggested that injury to the pulmonary capillary bed along with no stimulation of antioxidant enzymes or other protective enzymes may contribute to the enhanced susceptibility of H-S rats to the lethal effects of subsequent exposure to 100% O_2. Audi et al. (26) demonstrated a decrease in the activity of mitochondria complex I (51%) and complex IV (25%) in the lung tissue homogenate from H-S rats. They suggested that this mitochondrial change could alter lung tissue mitochondrial function and contribute to the susceptibility of H-S rats to lethal hyperoxia.

Previously, we proposed that tolerance of hyperoxia-induced ARDS is associated with the ability of the host to rapidly increase its lung antioxidant enzymes in response to hyperoxia exposure, or with an increase in the lung antioxidant content induced prior to and maintained during hyperoxia exposure (24). Exposure to hyperoxia for 48 h increased (~40%) glutathione (GSH) tissue content and this increase is maintained during the 24-h in room air (H-T) (Table 4) (26, 31). Such results suggest that increased lung tissue GSH, which protects sulfhydryl components of the mitochondrial ETC from oxidation (65–67), could be a factor in H-T tolerance. Audi et al. (26) reported a significantly smaller increase in lung tissue GSH concentration in H-S (19%) than H-T (40%) rats (Table 4). Frank et al. (13) suggested that tolerance of H-T rats is associated with increased lung antioxidant enzymes GSH peroxidase, superoxide dismutase, and catalase during reexposure of H-T rats to 100% O_2.

The results of the present study show that for H-T lungs, the decrease in complex I expression/activity, which is normally in excess, is accompanied by an increase in complex V expression and complex IV activity (Table 4), which could account for the increase in the capacity of *state 3* OxPhos for ATP synthesis and could decrease mitochondrial ROS production. These changes along with the relatively high tissue GSH content (Table 4) could protect mitochondria from additional stress such as exposure to >95% O_2. This would be consistent with the decrease in mt-DAMPs in plasma from H-T rats. For H-S lungs, results suggest that excess of complex I, which is the case in health, and a larger contribution of complex II to $\Delta\psi_m$ might be sufficient to overcome the effect of a decrease in complex I expression/activity and a decrease in RCR and *state 3* OxPhos capacity for ATP synthesis on $\Delta\psi_m$ in lungs. However, the higher dependency of lung tissue $\Delta\psi_m$ on complex II could lead to higher mitochondrial ROS production. Furthermore, complex I expression/activity is low enough that additional stress (e.g., exposure to >95% O_2), which further decreases complex I expression/activity, could deteriorate lung tissue mitochondria and have a significant effect on cellular functions. These changes in mitochondrial bioenergetics along with the increase in K_f could make H-S rats more susceptible to stress such as exposure to exposure to >95% O_2. These results are clinically relevant since exposure to hyperoxia is a primary therapy for patients with ARDS, and ventilation with $\geq$ 60% O_2 is often required for extended periods, particularly in subjects with COVID-19 (68). In addition, differential sensitivity to hyperoxia surely occurs in humans, given the wide spectrum of responses to a similar insult (15) and some variation in susceptibility to severe ARDS based on genetic polymorphisms (69).

APPENDIX

We used a previously developed physiologically based pharmacokinetic (PBPK) model that describes the pulmonary disposition of rhodamine 6G (R6G) for quantitative interpretation of the R6G data and for estimating lung tissue mitochondrial membrane potential ($\Delta\psi_m$) (23, 35). The model (Fig. 2) consists of four regions, namely the tubing connecting the reservoir to the pulmonary artery, lung vasculature, extravascular (intracellular, nonmitochondrial) region, and mitochondria, each with volume V_{tub}, V_c, V_e, and V_m, respectively. Within the vasculature, the model accounts for binding of R6G to BSA. The model also accounts for electrochemical gradients that drive the uptake of R6G from the vascular to the extravascular region and from there to the mitochondria region. Within the extravascular region, the model allows for slowly equilibrating interactions for R6G. Within the mitochondrial region, the model accounts for the binding of R6G to protein (35).

The volumes of the four regions, the dissociation constant for R6G binding to protein [bovine serum albumin (BSA)] in the vascular region (K_{d1}), the mitochondrial permeability-surface area product for R6G (P_2S_2), and the plasma membrane potential ($\Delta\psi_p$) were fixed to previously estimated values (35). In addition, the rate of efflux of R6G via Pgp pump from cytoplasm to the vascular region (K_{pgp}) was set to zero since the Pgp inhibitor verapamil was added to the perfusate for all three phases of the protocol in all experiments (35). Thus, for each lung the unknown model parameters are $\Delta\psi_m$, K_{d3}, $\hat{k}_2$, k_{2r}, and P_1S_1 (Table 2).

The rates of change in the concentrations of R6G in each of the four regions are described by the following system of ordinary differential equations (ODEs), which were derived using the laws of mass balance and mass action.

Tubing Region

$$V_{tub}\frac{d[C_{tub}]}{dt} = Q([C_{in}] - [C_{tub}]) \qquad (A1)$$

where $[C_{in}]$ and $[C_{tub}]$ are total (free + bound) concentration of R6G in reservoir and tubing regions, respectively, and Q is the pump flow rate.

Vascular Region

$$V_c \frac{d[\hat{C}_c]}{dt} = -S_1 J_1 + K_{pgp}[C_e] + Q\left([C_{tub}] - [\hat{C}_c]\right) \quad (A2)$$

where $[\hat{C}_c] = [C_c] + [C_c B_c] = [C_c]\left(1 + \frac{[B_c]}{K_{d1}}\right)$, K_{d1} is the R6G to BSA-binding dissociation constant, $[C_c]$ and $[C_c B_c]$ are the respective concentrations of free and BSA-bound R6G within the vascular region, S_1 is the vascular surface area, $J_1 = \frac{\alpha_{p_1}\Delta\psi_p}{(1-e^{-\alpha\Delta\psi_p})}\left(e^{-\alpha\Delta\psi_p}[C_c] - [C_e]\right)$, and $\alpha = ZF/RT$ is a constant dependent on the universal gas constant (R), Faraday constant (F), R6G valence ($Z = 1$), and absolute temperature (T).

Nonmitochondrial Region

Rates of change in the concentrations of free, $[C_e]$, and protein-bound, $[C_e B_e]$, R6G within this region are as follows:

$$Ve\frac{d[C_e]}{dt} = Ve\left(k_{2r}[C_e B_e] - \hat{k}_2[C_e]\right) - S_2 J_2 + S_1 J_1 - K_{pgp}[C_e] \quad (A3)$$

$$Ve\frac{d[C_e B_e]}{dt} = V_e\left(-k_{2r}[C_e B_e] + \hat{k}_2[C_e]\right) \quad (A4)$$

where $\hat{k}_2 = k_2[B_e]$, $[B_e]$ is the concentration of extravascular R6G-binding sites, S_2 is the mitochondrial surface area, and $J_2 = \frac{\alpha P_2 \Delta\psi_m}{(1-e^{-\alpha\Delta\psi_m})}\left(e^{-\alpha\Delta\psi_m}[C_e] - [C_m]\right)$.

Mitochondrial Region

Rate of change in the concentration of free R6G, $[C_m]$, within this region:

$$V_{m\_app}\frac{d[C_m]}{dt} = S_2 J_2 \quad (A5)$$

where $V_{m\_app} = Vm\left(1 + \frac{1}{K_{d3}}\right)$ is the apparent volume of the mitochondrial region, $K_{d3} = \frac{k_{3r}}{k_3[B_m]}$ is R6G and B_m-binding dissociation constant, and $[B_m]$ is the protein concentration within the mitochondrial region, and k_3 and k_{3r} are the association and dissociation rate constants of R6G-B_m binding in the mitochondrial region, respectively.

DATA AVAILABILITY

Data will be made available upon reasonable request.

SUPPLEMENTAL DATA

Supplemental Figs. S1–S6: https://doi.org/10.6084/m9.figshare.25992397.

ACKNOWLEDGMENTS

We appreciate the technical expertise of Sushma Kaul in preparation of the Western blot studies.

GRANTS

This work was supported by NIH 2R15HL129209-03 (to S.H. Audi, A.V. Clough, and E.R. Jacobs), VA Merit Review Award BX001681 (to E.R. Jacobs, S.H. Audi, and A.V. Clough), and NSF Grant DMS 2153387 (to R.K. Dash).

DISCLOSURES

No conflicts of interest, financial or otherwise, are declared by the authors.

AUTHOR CONTRIBUTIONS

P.T. and S.H.A. conceived and designed research; P.T., D.D.D., G.P.S., and S.H.A. performed experiments; P.T., D.D.D., R.K.D., and S.H.A. analyzed data; P.T., D.D.D., R.K.D., A.V.C., E.R.J., and S.H.A. interpreted results of experiments; P.T., E.R.J., and S.H.A. prepared figures; P.T. and S.H.A. drafted manuscript; P.T., D.D.D., R.K.D., G.P.S., A.V.C., E.R.J., and S.H.A. edited and revised manuscript; P.T., D.D.D., R.K.D., G.P.S., A.V.C., E.R.J., and S.H.A. approved final version of manuscript.

REFERENCES

1. **Bellani G**, **Laffey JG**, **Pham T**, **Fan E**, **Brochard L**, **Esteban A**, **Gattinoni L**, **van Haren F**, **Larsson A**, **McAuley DF**, **Ranieri M**, **Rubenfeld G**, **Thompson BT**, **Wrigge H**, **Slutsky AS**, **Pesenti A**; **ESICM Trials Group.** Epidemiology, patterns of care, and mortality for patients with acute respiratory distress syndrome in intensive care units in 50 countries. *JAMA* 315: 788–800, 2016. doi:10.1001/jama.2016.0291.
2. **Levitt JE**, **Matthay MA.** Clinical review: Early treatment of acute lung injury—paradigm shift toward prevention and treatment prior to respiratory failure. *Crit Care* 16: 223, 2012. doi:10.1186/cc11144.
3. **Kumar G**, **Kumar N**, **Taneja A**, **Kaleekal T**, **Tarima S**, **McGinley E**, **Jimenez E**, **Mohan A**, **Khan RA**, **Whittle J**, **Jacobs E**, **Nanchal R**; **Milwaukee Initiative in Critical Care Outcomes Research (MICCOR) Group of Investigators.** Nationwide trends of severe sepsis in the 21st century (2000-2007). *Chest* 140: 1223–1231, 2011. doi:10.1378/chest.11-0352.
4. **Honiden S**, **Gong MN.** Diabetes, insulin, and development of acute lung injury. *Crit Care Med* 37: 2455–2464, 2009. doi:10.1097/CCM.0b013e3181a0fea5.
5. **Fan E**, **Brodie D**, **Slutsky AS.** Acute respiratory distress syndrome: advances in diagnosis and treatment. *JAMA* 319: 698–710, 2018. doi:10.1001/jama.2017.21907.
6. **Stolmeijer R**, **Ter Maaten JC**, **Zijlstra JG**, **Ligtenberg JJ.** Oxygen therapy for sepsis patients in the emergency department: a little less? *Eur J Emerg Med* 21: 233–235, 2013. doi:10.1097/MEJ.0b013e328361c6c7.
7. **Ligtenberg JJ**, **Stolmeijer R**, **Broekema JJ**, **Ter Maaten JC**, **Zijlstra JG.** A little less saturation? *Crit Care* 17: 439, 2013. doi:10.1186/cc12726.
8. **Fisher AB**, **Beers MF.** Hyperoxia and acute lung injury. *Am J Physiol Lung Cell Mol Physiol* 295: L1066, 2008. doi:10.1152/ajplung.90486.2008.
9. **Kallet RH**, **Matthay MA.** Hyperoxic acute lung injury. *Respir Care* 58: 123–141, 2013. doi:10.4187/respcare.01963.
10. **Crapo JD**, **Tierney DF.** Superoxide dismutase and pulmonary oxygen toxicity. *Am J Physiol* 226: 1401–1407, 1974. doi:10.1152/ajplegacy.1974.226.6.1401.
11. **Frank L**, **Bucher JR**, **Roberts RJ.** Oxygen toxicity in neonatal and adult animals of various species. *J Appl Physiol Respir Environ Exerc Physiol* 45: 699–704, 1978. doi:10.1152/jappl.1978.45.5.699.
12. **Crapo JD**, **Barry BE**, **Foscue HA**, **Shelburne J.** Structural and biochemical changes in rat lungs occurring during exposures to lethal and adaptive doses of oxygen. *Am Rev Respir Dis* 122: 123–143, 1980. doi:10.1164/arrd.1980.122.1.123.
13. **Frank L**, **Iqbal J**, **Hass M**, **Massaro D.** New "rest period" protocol for inducing tolerance to high O2 exposure in adult rats. *Am J Physiol Lung Cell Mol Physiol* 257: L226–L231, 1989. doi:10.1152/ajplung.1989.257.4.L226.
14. **Hayatdavoudi G**, **O'Neil JJ**, **Barry BE**, **Freeman BA**, **Crapo JD.** Pulmonary injury in rats following continuous exposure to 60% O2

for 7 days. *J Appl Physiol Respir Environ Exerc Physiol* 51: 1220–1231, 1981. doi:10.1152/jappl.1981.51.5.1220.
15. **Capellier G**, **Maupoil V**, **Boussat S**, **Laurent E**, **Neidhardt A.** Oxygen toxicity and tolerance. *Minerva Anestesiol* 65: 388–392, 1999.
16. **Zhan B**, **Shen J.** Mitochondria and their potential role in acute lung injury (Review). *Exp Ther Med* 24: 479, 2022. doi:10.3892/etm.2022.11406.
17. **Reiss LK**, **Uhlig U**, **Uhlig S.** Models and mechanisms of acute lung injury caused by direct insults. *Eur J Cell Biol* 91: 590–601, 2012. doi:10.1016/j.ejcb.2011.11.004.
18. **Chow CW**, **Herrera Abreu MT**, **Suzuki T**, **Downey GP.** Oxidative stress and acute lung injury. *Am J Respir Cell Mol Biol* 29: 427–431, 2003. doi:10.1165/rcmb.F278.
19. **Kellner M**, **Noonepalle S**, **Lu Q**, **Srivastava A**, **Zemskov E**, **Black SM.** ROS signaling in the pathogenesis of acute lung injury (ALI) and acute respiratory distress syndrome (ARDS). *Adv Exp Med Biol* 967: 105–137, 2017. doi:10.1007/978-3-319-63245-2_8.
20. **Sanders AP**, **Baylin GJ.** A common denominator in the etiology of adult respiratory distress syndrome. *Med Hypotheses* 6: 951–965, 1980. doi:10.1016/0306-9877(80)90047-x.
21. **Sanders SP**, **Zweier JL**, **Kuppusamy P**, **Harrison SJ**, **Bassett DJ**, **Gabrielson EW**, **Sylvester JT.** Hyperoxic sheep pulmonary microvascular endothelial cells generate free radicals via mitochondrial electron transport. *J Clin Invest* 91: 46–52, 1993. doi:10.1172/JCI116198.
22. **Bongard RD**, **Yan K**, **Hoffmann RG**, **Audi SH**, **Zhang X**, **Lindemer BJ**, **Townsley MI**, **Merker MP.** Depleted energy charge and increased pulmonary endothelial permeability induced by mitochondrial complex I inhibition are mitigated by coenzyme Q1 in the isolated perfused rat lung. *Free Radic Biol Med* 65: 1455–1463, 2013. doi:10.1016/j.freeradbiomed.2013.07.040.
23. **Audi SH**, **Ganesh S**, **Taheri P**, **Zhang X**, **Dash RK**, **Clough AV**, **Jacobs ER.** Depolarized mitochondrial membrane potential and protection with duroquinone in isolated perfused lungs from rats exposed to hyperoxia. *J Appl Physiol (1985)* 132: 346–356, 2022. doi:10.1152/japplphysiol.00565.2021.
24. **Audi SH**, **Taheri P**, **Zhao M**, **Hu K**, **Jacobs ER**, **Clough AV.** In vivo molecular imaging stratifies rats with different susceptibilities to hyperoxic acute lung injury. *Am J Physiol Lung Cell Mol Physiol* 323: L410–L422, 2022 [Erratum in Am J Physiol Lung Cell Mol Physiol 324: L243, 2023]. doi:10.1152/ajplung.00126.2022.
25. **Gan Z**, **Roerig DL**, **Clough AV**, **Audi SH.** Differential responses of targeted lung redox enzymes to rat exposure to 60 or 85% oxygen. *J Appl Physiol (1985)* 111: 95–107, 2011. doi:10.1152/japplphysiol.01451.2010.
26. **Audi SH**, **Roerig DL**, **Haworth ST**, **Clough AV.** Role of glutathione in lung retention of 99mTc-hexamethylpropyleneamine oxime in two unique rat models of hyperoxic lung injury. *J Appl Physiol (1985)* 113: 658–665, 2012. doi:10.1152/japplphysiol.00441.2012.
27. **Beyer AM**, **Norwood Toro LE**, **Hughes WE**, **Young M**, **Clough AV**, **Gao F**, **Medhora M**, **Audi SH**, **Jacobs ER.** Autophagy, TERT, and mitochondrial dysfunction in hyperoxia. *Am J Physiol Heart Circ Physiol* 321: H985–H1003, 2021. doi:10.1152/ajpheart.00166.2021.
28. **Kumagai Y**, **Takeuchi O**, **Akira S.** TLR9 as a key receptor for the recognition of DNA. *Adv Drug Deliv Rev* 60: 795–804, 2008. doi:10.1016/j.addr.2007.12.004.
29. **Matute-Bello G**, **Downey G**, **Moore BB**, **Groshong SD**, **Matthay MA**, **Slutsky AS**, **Kuebler WM**; **Acute Lung Injury in Animals Study Group.** An official American Thoracic Society workshop report: features and measurements of experimental acute lung injury in animals. *Am J Respir Cell Mol Biol* 44: 725–738, 2011. doi:10.1165/rcmb.2009-0210ST.
30. **Madhu V**, **Boneski PK**, **Silagi E**, **Qiu Y**, **Kurland I**, **Guntur AR**, **Shapiro IM**, **Risbud MV.** Hypoxic regulation of mitochondrial metabolism and mitophagy in nucleus pulposus cells is dependent on HIF-1α-BNIP3 axis. *J Bone Miner Res* 35: 1504–1524, 2020. doi:10.1002/jbmr.4019.
31. **Audi SH**, **Jacobs ER**, **Zhang X**, **Camara AK**, **Zhao M**, **Medhora MM**, **Rizzo B**, **Clough AV.** Protection by inhaled hydrogen therapy in a rat model of acute lung injury can be tracked in vivo using molecular imaging. *Shock* 48: 467–476, 2017. doi:10.1097/SHK.0000000000000872.
32. **Bradford MM.** A rapid and sensitive method for the quantitation of microgram quantities of protein utilizing the principle of protein-dye binding. *Anal Biochem* 72: 248–254, 1976. doi:10.1006/abio.1976.9999.
33. **Tomar N**, **Zhang X**, **Kandel SM**, **Sadri S**, **Yang C**, **Liang M**, **Audi SH**, **Cowley AW Jr**, **Dash RK.** Substrate-dependent differential regulation of mitochondrial bioenergetics in the heart and kidney cortex and outer medulla. *Biochim Biophys Acta Bioenerg* 1863: 148518, 2022. doi:10.1016/j.bbabio.2021.148518.
34. **Chowdhury SR**, **Djordjevic J**, **Albensi BC**, **Fernyhough P.** Simultaneous evaluation of substrate-dependent oxygen consumption rates and mitochondrial membrane potential by TMRM and safranin in cortical mitochondria. *Biosci Rep* 36: e00286, 2015. doi:10.1042/BSR20150244.
35. **Audi SH**, **Cammarata A**, **Clough AV**, **Dash RK**, **Jacobs ER.** Quantification of mitochondrial membrane potential in the isolated rat lung using rhodamine 6G. *J Appl Physiol (1985)* 128: 892–906, 2020. doi:10.1152/japplphysiol.00789.2019.
36. **Audi SH**, **Clough AV**, **Haworth ST**, **Medhora M**, **Ranji M**, **Densmore JC**, **Jacobs ER.** 99MTc-hexamethylpropyleneamine oxime imaging for early detection of acute lung injury in rats exposed to hyperoxia or lipopolysaccharide treatment. *Shock* 46: 420–430, 2016. doi:10.1097/SHK.0000000000000605.
37. **Edwards A**, **Palm F**, **Layton AT.** A model of mitochondrial O(2) consumption and ATP generation in rat proximal tubule cells. *Am J Physiol Renal Physiol* 318: F248–F259, 2020. doi:10.1152/ajprenal.00330.2019.
38. **Divakaruni AS**, **Jastroch M.** A practical guide for the analysis, standardization and interpretation of oxygen consumption measurements. *Nat Metab* 4: 978–994, 2022. doi:10.1038/s42255-022-00619-4.
39. **Sommer SP**, **Sommer S**, **Sinha B**, **Walter D**, **Aleksic I**, **Gohrbandt B**, **Otto C**, **Leyh RG.** Glutathione preconditioning ameliorates mitochondria dysfunction during warm pulmonary ischemia-reperfusion injury. *Eur J Cardiothorac Surg* 41: 140–148, 2012. doi:10.1016/j.ejcts.2011.02.081.
40. **Sadri S**, **Tomar N**, **Yang C**, **Audi SH**, **Cowley AW Jr**, **Dash RK.** Effects of ROS pathway inhibitors and NADH and FADH(2) linked substrates on mitochondrial bioenergetics and ROS emission in the heart and kidney cortex and outer medulla. *Arch Biochem Biophys* 744: 109690, 2023. doi:10.1016/j.abb.2023.109690.
41. **Sadri S**, **Zhang X**, **Audi SH**, **Cowley AW Jr**, **Dash RK.** Computational modeling of substrate-dependent mitochondrial respiration and bioenergetics in the heart and kidney cortex and outer medulla. *Function (Oxf)* 4: zqad038, 2023. doi:10.1093/function/zqad038.
42. **Carlson DE**, **Pumplin DW**, **Ghavam S**, **Fiedler SM**, **Chiu WC**, **Scalea TM.** ATP accelerates respiration of mitochondria from rat lung and suppresses their release of hydrogen peroxide. *J Bioenerg Biomembr* 37: 327–338, 2005. doi:10.1007/s10863-005-8644-3.
43. **Barrientos A**, **Moraes CT.** Titrating the effects of mitochondrial complex I impairment in the cell physiology. *J Biol Chem* 274: 16188–16197, 1999. doi:10.1074/jbc.274.23.16188.
44. **Campian JL**, **Qian M**, **Gao X**, **Eaton JW.** Oxygen tolerance and coupling of mitochondrial electron transport. *J Biol Chem* 279: 46580–46587, 2004. doi:10.1074/jbc.M406685200.
45. **Li J**, **Gao X**, **Qian M**, **Eaton JW.** Mitochondrial metabolism underlies hyperoxic cell damage. *Free Radic Biol Med* 36: 1460–1470, 2004. doi:10.1016/j.freeradbiomed.2004.03.005.
46. **Long G**, **Gong R**, **Wang Q**, **Zhang D**, **Huang C.** Role of released mitochondrial DNA in acute lung injury. *Front Immunol* 13: 973089, 2022. doi:10.3389/fimmu.2022.973089.
47. **Sun S**, **Sursal T**, **Adibnia Y**, **Zhao C**, **Zheng Y**, **Li H**, **Otterbein LE**, **Hauser CJ**, **Itagaki K.** Mitochondrial DAMPs increase endothelial permeability through neutrophil dependent and independent pathways. *PLoS One* 8: e59989, 2013. doi:10.1371/journal.pone.0059989.
48. **Zhang X**, **Dash RK**, **Jacobs ER**, **Camara AKS**, **Clough AV**, **Audi SH.** Integrated computational model of the bioenergetics of isolated lung mitochondria. *PLoS One* 13: e0197921, 2018. doi:10.1371/journal.pone.0197921.
49. **Fisher AB.** Functional evaluation of lung mitochondria. *Chest* 67: 24s–26s, 1975. doi:10.1378/chest.67.2_supplement.24s.
50. **Hirata T**, **Fukuse T**, **Hanaoka S**, **Matsumoto S**, **Chen Q**, **Wada H.** Mitochondrial respiration as an early marker of viability in cardiac-arrested rat lungs. *J Surg Res* 96: 268–276, 2001. doi:10.1006/jsre.2000.6079.
51. **Freeman BA**, **Crapo JD.** Hyperoxia increases oxygen radical production in rat lungs and lung mitochondria. *J Biol Chem* 256: 10986–10992, 1981.

52. **Bassett DJ**, **Elbon CL**, **Reichenbaugh SS.** Respiratory activity of lung mitochondria isolated from oxygen-exposed rats. *Am J Physiol Lung Cell Mol Physiol* 263: L439–L445, 1992. doi:10.1152/ajplung.1992.263.4.L439.
53. **Quarrie R**, **Cramer BM**, **Lee DS**, **Steinbaugh GE**, **Erdahl W**, **Pfeiffer DR**, **Zweier JL**, **Crestanello JA.** Ischemic preconditioning decreases mitochondrial proton leak and reactive oxygen species production in the postischemic heart. *J Surg Res* 165: 5–14, 2011. doi:10.1016/j.jss.2010.09.018.
54. **Divakaruni AS**, **Brand MD.** The regulation and physiology of mitochondrial proton leak. *Physiology (Bethesda)* 26: 192–205, 2011. doi:10.1152/physiol.00046.2010.
55. **Scialò F**, **Fernández-Ayala DJ**, **Sanz A.** Role of mitochondrial reverse electron transport in ROS signaling: potential roles in health and disease. *Front Physiol* 8: 428, 2017. doi:10.3389/fphys.2017.00428.
56. **Chance B**, **Hollunger G.** The interaction of energy and electron transfer reactions in mitochondria. I. General properties and nature of the products of succinate-linked reduction of pyridine nucleotide. *J Biol Chem* 236: 1534–1543, 1961.
57. **O'Neil JJ**, **Sanford RL**, **Wasserman S**, **Tierney DF.** Metabolism in rat lung tissue slices: technical factors. *J Appl Physiol Respir Environ Exerc Physiol* 43: 902–906, 1977. doi:10.1152/jappl.1977.43.5.902.
58. **Fisher AB.** Intermediary metabolism of the lung. *Environ Health Perspect* 55: 149–158, 1984. doi:10.1289/ehp.8455149.
59. **Audi SH**, **Friedly N**, **Dash RK**, **Beyer AM**, **Clough AV**, **Jacobs ER.** Detection of hydrogen peroxide production in the isolated rat lung using Amplex red. *Free Radic Res* 52:1052–1062, 2018. doi:10.1080/10715762.2018.1511051.
60. **Audi SH**, **Bongard RD**, **Dawson CA**, **Siegel D**, **Roerig DL**, **Merker MP.** Duroquinone reduction during passage through the pulmonary circulation. *Am J Physiol Lung Cell Mol Physiol* 285: L1116–L1131, 2003. doi:10.1152/ajplung.00185.2003.
61. **Hadrava Vanova K**, **Kraus M**, **Neuzil J**, **Rohlena J.** Mitochondrial complex II and reactive oxygen species in disease and therapy. *Redox Rep* 25: 26–32, 2020. doi:10.1080/13510002.2020.1752002.
62. **Thaete LG**, **Malkinson AM.** Differential staining of normal and neoplastic mouse lung epithelia by succinate dehydrogenase histochemistry. *Cancer Lett* 52: 219–227, 1990. doi:10.1016/0304-3835(90)90190-9.
63. **Herrero R**, **Sanchez G**, **Lorente JA.** New insights into the mechanisms of pulmonary edema in acute lung injury. *Ann Transl Med* 6: 32, 2018. doi:10.21037/atm.2017.12.18.
64. **Piantadosi CA**, **Suliman HB.** Mitochondrial dysfunction in lung pathogenesis. *Annu Rev Physiol* 79: 495–515, 2017. doi:10.1146/annurev-physiol-022516-034322.
65. **Deneke SM**, **Lynch BA**, **Fanburg BL.** Transient depletion of lung glutathione by diethylmaleate enhances oxygen toxicity. *J Appl Physiol (1985)* 58: 571–574, 1985. doi:10.1152/jappl.1985.58.2.571.
66. **Djurhuus R**, **Svardal AM**, **Thorsen E.** Glutathione in the cellular defense of human lung cells exposed to hyperoxia and high pressure. *Undersea Hyperb Med* 26: 75–85, 1999.
67. **Suttorp N**, **Toepfer W**, **Roka L.** Antioxidant defense mechanisms of endothelial cells: glutathione redox cycle versus catalase. *Am J Physiol Cell Physiol* 251: C671–C680, 1986. doi:10.1152/ajpcell.1986.251.5.C671.
68. **Chang R**, **Elhusseiny KM**, **Yeh YC**, **Sun WZ.** COVID-19 ICU and mechanical ventilation patient characteristics and outcomes—a systematic review and meta-analysis. *PLoS One* 16: e0246318, 2021. doi:10.1371/journal.pone.0246318.
69. **Reddy AJ**, **Kleeberger SR.** Genetic polymorphisms associated with acute lung injury. *Pharmacogenomics* 10: 1527–1539, 2009. doi:10.2217/pgs.09.89.